International
Progress Report

IPR-01-59

Äspö Hard Rock Laboratory

TRUE Block Scale project
Tracer test stage

Mineralogical and geochemical analyses of fracture filling materials (gouge and coutings) from drillcore samples

Berta de la Cruz
Ana M. Fernández
Pedro Rivas
Juan Cózar
Miguel A. Labajo

CIEMAT, Spain

June 2000

Svensk Kärnbränslehantering AB
Swedish Nuclear Fuel
and Waste Management Co
Box 5864
SE-102 40 Stockholm Sweden
Tel +46 8 459 84 00
Fax +46 8 661 57 19

Äspö Hard Rock
Laboratory

Report no.	No.
IPR-01-59	F56K
Author	Date
B de la Cruz, A M Rivas, J Cózar, M A Labajo	00-06-01
Checked by	Date
Anders Winberg	00-12-01
Approved	Date
Christer Svemar	02-08-23

Äspö Hard Rock Laboratory

TRUE Block Scale project
Tracer test stage

Mineralogical and geochemical analyses of fracture filling materials (gouge and coutings) from drillcore samples

Berta de la Cruz
Ana M. Fernández
Pedro Rivas
Juan Cózar
Miguel A. Labajo

CIEMAT, Spain

June 2000

Keywords: Fracture filling, porosity, CEC, mineralogy, geochemistry

Abstract

The mineralogical and geochemical characterization of coatings and gouge material corresponding to structures # 20 and 22 from borehole KI0025F03, structure # 13 from KI0025F02 and KI0025F03 and # 6 intersecting boreholes KI0025F03 and KA2563A has been carried out, in order to aid in the study of tracer transport and retention. Density, water adsorption, porosity (calculated from the former two) and the cation exchange capacity (CEC) were also determined in gouge material.

The intersections of the same structure with different boreholes show significant mineralogical and textural differences. The only clay minerals present in significant amounts are chlorite and illite. However, saponite has been identified in coatings, though in very scarce amounts, probably due to loss during drilling.

Density is mainly related to the Fe and Ca contents which are represented by Fe-bearing minerals, and, partially, by epidote, respectively. The highest values of water adsorption, porosity and CEC are associated with the highest contents of phyllosilicates.

Sammanfattning

Den mineralogiska och geokemiska karakteriseringen av sprickmineral och gougematerial i struktur #20 och 22 från borrhål KI0025F03, struktur #13 från KI0025F02 och KI0025F03 och #6 i borrhål KI0025F03 och KA2563A, har utförts i syfte att stödja studier om spårämnestransport och retention. Densitet, vattenadsorption, porositet (beräknad från de föregående två), och katjonbyteskapaciteten (CEC) bestämdes också i gougematerialet.

Genomskärningarna av samma struktur med olika borrhål visar signifikanta skillnader i mineralogi och textur. De enda lermineralen som återfinns i signifikant mängd är klorit och illit. I övrigt har saponit identifierats i sprickbeklädnader i väldigt små mängder, troligen p g a bortspolning vid borrning.

Densiteten är huvudsakligen relaterat till Fe- och Ca-innehållet som är representerat av Fe-bärande mineral, respektive delvis av epidot. De högsta värdena av vattenadsorption, porositet och CEC kan kopplas till det högsta innehållet av phyllosilikater.

Contents

Abstract **i**

Contents **ii**

List of Figures **iv**

List of Tables **v**

1 Introduction **1**

2 Sampling and sample preparation **2**

2.1 Sampling 2

2.2 Preparation of samples 2
2.2.1 Coatings 3
2.2.2 Gouge material 3
2.2.3 Wall rock 4

3 Analytical techniques **5**

3.1 Mineralogical and chemical composition 5
3.1.1 Thin sections 5
3.1.2 SEM analyses 5
3.1.3 XRD 5
3.1.4 Chemical analyses 5

3.2 Physical parameters 7

3.3 Physico-chemical parameters 8

3.4 Isotope Analyses 8
3.4.1 Stable isotopes (^{13}C, ^{18}O) 8
3.4.2. Radioactive isotopes 10

4 Chemical composition **11**

5 Mineralogical composition and petrographic studies **13**

5.1 Mineralogical composition 13

5.2 Petrographic study 21
5.2.1 Structure # 6 21
5.2.2 Structure # 13 23
5.2.3 Structure # 22 25
5.2.4 Structure # 20 27

5.3	Discussion of results	28
6	**Isotope studies**	**30**
6.1	Stable isotopes	30
6.2	Radioactive isotopes	31
7	**Physico-chemical parameters**	**33**
8	**Cation Exchange Capacity (CEC)**	**35**
9	**Comparison of physico-chemical parameters and CEC in the different structures**	**38**
9.1	Structure # 6	38
9.2	Structure # 22	38
9.3	Structure # 20	38
9.4	Structure # 13	39
10	**Conclusions**	**40**
Acknowledgement		**41**
References		**42**

ANNEX A	Photo documentation of samples
ANNEX B	Petrographic microphotographs
ANNEX C	SEM microphotographs

List of Figures

Figure 5-1 XRD, borehole KI0025F03/51.9 m/# 6 14

Figure 5-2 XRD, borehole KI0025F03/63.2 m/# 22 14

Figure 5-3 XRD, borehole KI0025F03/73.1 m/# 20 15

Figure 5-4 XRD, borehole KI0025F03/87.9 m/# 13 15

Figure 5-5 XRD, borehole KI0025F02/ 93.9 m/ # 13 16

Figure 5-6 XRD, borehole KI0025F/ 88.8 m/ # 22 16

Figure 5-7 XRD, borehole KA2563A/ 154 m/ # 6 17

Figure 5-8 XRD of oriented aggregates. Smectite was only confirmed in **c** 19

Figure 7- 1 Correlation between Density and Total Fe_2O_3 34

Figure 8- 1 Correlation between CEC and Al_2O_3 of gouge fragments 37

List of Tables

Table 2- 1 Samples collected from boreholes KI0025F03, KI0025F02, KI0025F and KA2563A 2

Table 2- 2 Weight of coatings 3

Table 2- 3 Sieving of gouge material. Weight of each fraction (g) 3

Table 3- 1 Types of material and analyses performed 6

Table 4- 1 Chemical composition of gouge fragments. Major elements (%) 12

Table 4- 2 Chemical composition of gouge fragments. Minor elements (ppm) 12

Table 5- 1 Reference intensity ratio (RIR) 17

Table 5-2 Semiquantitative composition (XRD) (%) 18

Table 5- 3 Mineralogical and petrographic comparison of rock, gouge and coatings of structure # 6 22

Table 5- 4 Mineralogical and petrographic differences in the intersection points of structure # 6 22

Table 5- 5 Mineralogical and petrographic comparison of rock, gouge and coatings of structure #13 24

Table 5- 6 Mineralogical and petrographic differences in the intersection points of structure #13 25

Table 5- 7 Mineralogical and petrographic comparison of rock, gouge and coatings of structure #22 26

Table 5- 8 Mineralogical and petrographic differences in the intersection points ofstructure #22 27

Table 5- 9 Petrographic study of structure #20 in KI0025F03 at 73.1 m 28

Table 6- 1 Isotopic signature of calcites from fracture fillings and gouge 30

Table 6- 2 Radioactive isotopes 32

Table 7- 1 Physical characteristics of the samples 33

Table 8- 1 Soluble salts obtained in the generic rock material from a distilled water solution at 1:10 solid to liquid ratio 35

Table 8- 2 Soluble salts obtained in the generic rock material from an alcoholic solution (60% ethanol/distilled water) at 1:5 solid to liquid ratio 36

Table 8- 3 Cation exchange capacity obtained in the generic rock material 37

ANNEX A PHOTO DOCUMENTATION OF SAMPLES

Fig. 1. KA2563/ 154 m/#6
Fig. 2. KI0025F03/ 51.9 m/#6
Fig. 3. KI0025F03/ 63.2 m/#22
Fig. 4. KI0025F03/ 63.2 m/#22. Calcite coating.
Fig. 5. KI0025F03/ 73.1 m/#20
Fig. 6. KI0025F03/ 73.1 m/#20. Calcite macrocrystal in coating.
Fig. 7. KI0025F03/ 87.5 m/#21
Fig. 8. KI0025F/ 88.8 m/#22
Fig. 9. KI0025F02/ 93.9 m/#13

ANNEX B PETROGRAPHIC MICROPHOTOGRAPHS

Fig. 1 BOREHOLE KI0025F03/ 51.9m / #6. a) General aspect of cataclastic Äspö diorite: 1) epidote; 2) plagioclase. Crossed nicols, x12. **b)** Biotite totally altered to chlorite (1) with opaques (3) from biotite along cleavages; epidote (4) associated with chlorite. Plagioclase (2) slightly altered to sericite. Natural light, x100. **c)** Idiomorphic sphene (1) with alteration rims of Ti oxide (anatase, 2). Chlorite (3). Crossed nicols, x50. **d)** Fissural calcite (2) cutting recrystallized quartz (1). Crossed nicols, x50. **e)** General aspect of gouge fragment. Sericitized plagioclase (1), recrystallized quartz (2), chlorite (3) and epidote (4). Crossed nicols, x50.

Fig. 2. BOREHOLE KA2563A / 154m / #6. Gouge fragments. a) General aspect. Plagioclase (1). Fine-grained epidote-chlorite (2). Crossed nicols, x50; **b)** Lenticle of recrystallized quartz (1). Crossed nicols, x50. **c)** Altered Na-Ca plagioclase (1, only flakes of sericite (2) remain in some plagioclases). Crossed nicols, x50.

Fig. 3. BOREHOLE KI0025F03/ 87.5m / #13. a) General aspect of tectonized zone with slightly altered plagioclase (1). Bands of epidote-chlorite (2) are observed. Crossed nicols, x50. **b)** Chlorite formed by alteration of biotite. The heavy metal inclusions of biotite are still observed along the cleavage planes. Crossed nicols, x50. **c)** Zone (1) of opaques and Ti oxides surrounded by carbonate halo (2). Crossed nicols, x50. **d)** Gouge fragment showing altered plagioclase (1), in which only sericite flakes (yellow) remain in some of them. Crossed nicols, x50.

Fig. 4. BOREHOLE KI0025F02/ 93.9 m/ #13. a) General aspect of mylonite. K-feldspar (2), plagioclase (3) and poikilitic muscovite (1) are the main minerals. Crossed nicols, x50. **b)** Calcite (1) fills void and replaces muscovite (2). Crossed nicols, x50.

Fig. 5. BOREHOLE KI0025F03/ 63.2m / #22. a) General aspect of a mylonite, fine-grained bands (1) alternating with coarser bands (2). Crossed nicols, x12; **b)** Opaques (1) surrounded by carbonates (2). Chlorite (3) formed by alteration of biotite. Natural light, x50; **c)** General aspect of a gouge fragment mainly formed by fine-grained idiomorphic-subidiomorphic epidote (bright yellow) and chlorite (brown spots), both from alteration of biotite. Crossed nicols, x50.

Fig. 6. BOREHOLE KI0025F/ 88.8 m/ #22. a) Äspö diorite with slightly sericitized plagioclase (1) macrocrystal. Crossed nicols, x12; **b)** General aspect of a gouge fragment with K-feldspars (1) and plagioclase (2). Crossed nicols, x12; **c)** Kinks (1) formed in chlorite (from alteration of biotite), indicating the strong deformation undergone by these rocks. Crossed nicols, x50.

Fig. 7. BOREHOLE KI0025F03/ 73.1m / #20. a) Fine-grained bands formed by epidote (1 a) and microcrystalline plagioclase (1b). These bands adapt themselves to plagioclase (2) macrocrystals. Frequent opaques. Crossed nicols, x12; **b)** Detail of plagioclase (1) in the coarser-grained bands. Crossed nicols, x50; **c)** General aspect of a gouge fragment. Plagioclase (1) and abundant epidote (2). Crossed nicols, x50.

ANNEX C SEM MICROPHOTOGRAPHS

Fig. 1. a) BOREHOLE KI0025F03/ 51.9 m/ #6. Chlorite in gouge. b) BOREHOLE KA2563A/ 154m / #6. Gouge fragment. Collophorm Fe oxi-hydroxides (1) surrounded by a complex silicate compound with Mg, Ca and Fe (2). (1) and (2) have Cl probably from the evaporation of marine waters. Quartz (3).

Fig. 2. KI0025F03/ 87.9 m/ #13. COATING. a, b) Chlorite tranformed into Mg-rich smectite (saponite). **a-1, b-1**: EDX spectrum of saponite; **a-2, b-2**: EDX spectrum of chlorite.

Fig. 3. KI0025F03/ 87.9 m/ #13. COATING. a) Chlorite altered to saponite**; b)** General aspect of saponite.

Fig. 4. **KI0025F03/ 87.9 m/ #13. COATING.** General aspect **(a)** and detail **(b)** of illite. **c)** EDX spectrum of illite.

Fig. 5. **KI0025F03/ 87.9 m/ #13. COATING. a.** Pyrite (1) included in chlorite-calcite mass (2, 3); calcite (4). **b)** Pyrite (1) embedded in a mixture of biotite-calcite (3), which is partially transformed into chlorite-calcite (2); **b-1, b-2**: EDX spectrum of (2) and (3).

Fig. 6. KI0025F02/ 93.9 m/ #13. COATING. a. calcite **b.** (1) calcite; (2) epidote; (3) K-feldspar; (4) chlorite**. c.** (1) K-feldspar + graphite; (2) biotite. **d**. (1) plagioclase; (2) apatite; (3) calcite. 1) quartz; (2) pyrite; (3) calcite; (4) muscovite-biotite. **f.** (1) U oxide (Pb); (2) K-feldspar; (3) epidote; (4) chlorite.

Fig. 7. KI0025F03/ 88.8 m/ #22. a. COATING. Cromite (1) and K-feldspar (2); **b. GOUGE**. (1) Fe oxi-hydroxides; (2)calcite; (3) chlorite; (4) plagioclase; (5) quartz **c.** Detail aspect of b**. d. GOUGE.** (1) biotite; (2) epidote; 3) sphene. **e. GOUGE**. (1) chalcopyrite; (2) calcite; (3) plag; (4) epidote; (5) quartz. **f. GOUGE.** (1) pyrite; (2) quartz; (3) chlorite; K-feldspar.

Fig. 8. KI0025F03/ 73.1 m/ #22. GOUGE. a. Idiomorphic fluorite (1), pyrite(2), K-feldspar (3), quartz (4), Fe oxi-hydroxide(5); **b.** Probable remobilization of zircon(1); chlorite (2) associated with epidote (3), Na-plagioclase (4); **c.** Collophorm Fe oxi-hydroxides (1, 2) with Cl from evaporation of marine water, quartz (3) and epidote (4); d. Subidiomorphic quartz (1) with epidote and chlorite (2 and 4) and subidiomorphic plagioclase (3).

Fig. 9. KI0025F03 / 87.5 m/ #13. GOUGE. a) Spheres of Fe oxi-hydroxides (1) with plagioclase(2), epidote (3) and chlorite (4) and associated with biotite-chlorite (2) in **b. c)** calcite (1) and chlorite (2); **d)** calcite (2) covering smectite (3), Zn oxides present (1).

1 Introduction

The TRUE Block Scale Project tries to increase the understanding of the behavior of reactive and non-reactive tracers within a fracture network. For this purpose, the Tracer Test Stage is the final part of the experimental work being performed in the TRUE Block Scale Project, conducted at Äspö HRL. The site characterization data have identified several major hydraulically conductive structures, which have been intersected by several boreholes. The structural model, together with the hydraulic model, provides a basis for designing the geometry of the tests, in order to study tracer transport and retention.

The planned tracer tests will be carried out in a fracture network constituted by structures #13, #20 and #6, which are connected by #21 and #22, as determined by the reconciled March ´99 structural model. These structures were intersected by boreholes KI0025F02, KA2563A and KI0023B, and samples from each structure have already been characterized from a mineralogical and geochemical point of view (Tullborg, 1999 a, b; Tullborg, 1998). In early autumn 1999, a new borehole, KI0025F03, was drilled between KI0023B and KI0025F02, to validate these structures and the features that connect structures # 13, # 6 and # 20, as well as to further refine the structural model.

The objective of the present study, which has been carried out by CIEMAT, is to perform the mineralogical and geochemical characterization of the infill materials (gouge and coatings) of structure # 6, 20 and 21 from borehole KI0025F03, structure # 13 in KI0025F02, # 6 in KA2563A and # 22 in KI0025F. Furthermore the cation exchange capacity (CEC) will be determined in all the gouge materials.

The results will be integrated in the structural model and the ongoing studies, which will support the performance of the tracer tests.

2 Sampling and sample preparation

2.1 Sampling

The sampling was done in January 19, 2000 at Äspö HRL together with Eva-Lena Tullborg and Anders Winberg. Table 2- 1 shows the samples collected. A 10-cm long wall rock sample was collected in each structure.

Table 2- 1 Samples collected from boreholes KI0025F03, KI0025F02, KI0025F and KA2563A

BOREHOLE	DEPTH (m)	STRUCTURE ID	TYPE OF MATERIAL SAMPLED	LITHOLOGY
KI0025F03	51.9	6	R, G	ÄD
KI0025F03	63.2	22	R, G	Mylonite in diorite
KI0025F03	73.1	20	R,G	Mylonite
KI0025F03	87.9	13	R, G	Tectonized zone in ÄD with fine-grained granite
KI0025F02	93.9	13	R	Mylonite in altered ÄD
KI0025F	88.8	22	R, G	Altered ÄD
KA2563A	154	6	G	Fine-grained loose gouge

Annex A shows the pictures of the original samples collected.

2.2 Preparation of samples

There are three types of materials in the collected samples: coatings, gouge and wall rock.

2.2.1 Coatings

Coatings were scraped off from the structure surface with a knife and weighed (Table 2- 2). These samples, without grinding, were used for X-ray diffraction (XRD). Scanning electron microscope (SEM) studies were carried out in those samples where small splinters of coating could be scraped off, in order to know the textural relationship among minerals. Chemical analyses of these coatings could not be done due to their scarce amount. Calcite crystals were carefully scraped off from the structure surface and sent for stable isotopes (^{18}O, ^{13}C) analyses.

Table 2- 2 Weight of coatings

BOREHOLE; depth; structure ID	WEIGHT OF COATING (g)
KI0025F03; 51.9 m; #6	0.6
KI0025F03; 63.2m; #22	0.6
KI0025F03; 73.1 m; #20	0.1
KI0025F03; 87.9 m; #13	2.2
KI0025F02; 93.9 m; #13	0.5
KI0025F; 88.8 m; #22	1.2
KA2563A; 154m; #6	No coating

2.2.2 Gouge material

Gouge material was present in all the samples except those from KI0025F02. It was sieved dry (>1mm, 0.5 mm, 0.25 mm, 0.125 mm, 0.063 mm and < 0.063mm), and each fraction was weighed (Table 2- 3).

Table 2- 3 Sieving of gouge material. Weight of each fraction (g)

BOREHOLE	> 1 mm	0.5 mm	0.25 mm	0.125 mm	0.063 mm	< 0.063 mm
KI0025F03 51.9 m; #6	13.22	0.3	0.05	-	-	-
KI0025F0363.2 m; #22	40.43	0.5	0.3	0.2	-	-
KI0025F03 73.1m; #20	82.98	0.2	0.1	0.1	-	-
KI0025F03 87.9m; #13	52.31	0.1	0.1	-	-	-
KI0025F02 93.9 m; #13	-	-	-	-	-	-
KI0025F; 88.8m; #22	114.5	-	-		-	-
KA2563A 154m; #6	76.13	4	4.3	1.9	4.4	7.4

The amount of material in the < 1 mm fractions was very scarce (Table 2- 3), except in borehole KA2563A, in which the < 1mm material was abundant and could be sieved into 5 fractions. The natural fraction < 0.063mm from this borehole was used for chemical analyses, XRD, cation exchange capacity (CEC) and U series, in order to compare the results with the > 1 mm gouge material of this borehole, which was ground to < 0.063 mm.

Several fragments from the > 1 mm fraction were collected for thin sections, SEM and water adsorption porosity determinations. Other fragments were kept aside in case they were needed to complete any additional study. The remaining >1 mm gouge material (approximately half the original weight) from all the samples was ground dry to < 0.063 mm, and was used for chemical analyses, CEC, XRD and U series.

2.2.3 Wall rock

Slices of the wall rock were cut perpendicular to the structure surface for thin sections and studied by optical microscopy.

3 Analytical techniques

The different techniques applied to each type of sample are shown in Table 3- 1.

3.1 Mineralogical and chemical composition

3.1.1 Thin sections

The wall rock and gouge fragments were studied by thin sections (TS) dyed for K-feldspar and carbonate analyses at the Universidad Complutense de Madrid.

3.1.2 SEM analyses

SEM analyses of gouge fragments and coating splinters were carried out in a Zeiss DSM 960 digital scanning microscope coupled to a Link X-ray dispersive energy analyzer (SEM+EDX) at CIEMAT.

3.1.3 XRD

X-ray diffraction was carried out with a Phillips diffractometer, model PW 1840, using CuKα radiation at the Universidad Complutense de Madrid. In order to minimize preferred orientations, powders for diffraction were prepared in cavity mount and leveled off by knife edge without pressing. The accuracy of the method is controlled by making 5 measures per sample and calculating the standard deviation. The international ASTM tables were used for the qualitative interpretation of the X-ray patterns. All the determinations were carried out with an Al sample holder, except the coating corresponding to KI0025F03 at 73.1m, which was done with a Si sample holder due to insufficient amount of sample. For this reason, this analysis cannot be compared with the rest.

3.1.4 Chemical analyses

Table 3- 1 Types of material and analyses performed

BOREHOLE; Depth; structure ID	THIN SECTION	SEM	CEC+POROSITY *	CHEMICAL ANALYSES *	U SERIES *	XRD	STABLE ISOTOPES
KI0025F03; 51.9 m; #6	Wall rock + gouge > 1mm	Gouge fragment > 1mm	Gouge fragment > 1mm and ground gouge (< 0.063 mm)	ground gouge (< 0.063 mm)	ground gouge (< 0.063 mm)	Scraped coating Ground gouge (< 0.063 mm)	Calcite crystals scraped from coating
KI0025F03; 63.2 m; #22	Wall rock + gouge > 1mm	Gouge fragment > 1mm	Gouge fragment > 1mm and ground gouge	ground gouge (< 0.063 mm)	ground gouge (< 0.063 mm)	Scraped coating Ground gouge (< 0.063 mm)	
KI0025F03; 73.1 m; #20	Wall rock + gouge > 1mm	Gouge fragment > 1mm with calcite	Gouge fragment > 1mm and ground gouge	ground gouge (< 0.063 mm)	ground gouge (< 0.063 mm)	Scraped coating Ground gouge (< 0.063 mm)	Calcite macrocrystal scraped from coating
KI0025F03; 87.5m; #13	Wall rock + gouge > 1mm	Gouge fragment > 1mm Coating splinter	Gouge fragment > 1mm and ground gouge	ground gouge (< 0.063 mm)	ground gouge (< 0.063 mm)	Scraped coating Ground gouge (< 0.063 mm)	
KI0025F02; 93.9m; #13	Wall rock	Coating splinter	No gouge	No gouge	No gouge	Scraped coating	
KI0025F; 88.8 m; #22	Wall rock + gouge > 1mm	Gouge fragment > 1mm Coating splinter	Gouge fragment > 1mm and ground gouge	ground gouge (< 0.063 mm)	ground gouge (< 0.063 mm)	Scraped coating Ground gouge (< 0.063 mm)	Calcite crystals scraped from gouge fragments
KA2563A; 154 m; #6	Gouge > 1 mm	Gouge fragment > 1mm	Gouge fragment > 1mm and ground and natural gouge	Natural and ground gouge (< 0.063 mm)	ground gouge (< 0.063 mm)	Natural and ground gouge (< 0.063 mm)	

* only done with gouge fragments; not enough sample from coatings.

Solid phase

The chemical analyses for Al_2O_3, Fe_2O_3, MgO, MnO, TiO_2, CaO, P_2O_5, Ag, As, Ba, Be, Ce, Co, Cr, Cu, La, Mo, Ni, Sr, V, W, Y and Zn were carried out by inductively coupled plasma atomic emission spectrometry and inductively coupled plasma mass spectrometry, depending on the amount of sample (ICP-AES; ICP-MS); Na by flame atomic emission spectroscopy (FAES); SiO_2 and K by X-R fluorescence; U by laser kinetic fosforescence. A Leco CS-244 elemental analyzer was used for C and S, selective ion electrode for F and thermogravimetric analysis (TG) for H_2O^- and H_2O^+. All these techniques were performed at CIEMAT, except the X-R fluorescence which was done at the Instituto Tecnológico y Geominero de España.

Aqueous extracts

The soluble salts were analyzed in an aqueous extract solution. Ground gouge samples (<0.063 mm) were kept in contact with de-ionized water at 1:10 solid to liquid ratio (1g/10ml) and allowed to react for 1 hour. This was done in an anaerobic glove chamber. After phase separation by centrifuging, the supernatant solutions were analyzed.

The total alkalinity of the samples (expressed in mg/l of HCO_3^-) was determined by potenciometry with a Metrohm 682 titrator. The pH was determined with an Orion EA 920 pH-meter and the conductivity with an Orion 115 conductivity meter.

The major and trace elements: B, Ba, Bi, Ca, Cd, Co, Cr, Cu, Fe_{total}, Mg, Mn, Mo, Na, Ni, Pb, Sr, Ti, V and Zn were determined by ICP-AES using a Perkin-Elmer Elan 5000 spectrometer. Na^+ and K^+ were analyzed by flame atomic emission spectrometry (AAS-Flame) with a Perkin Elmer 2280 spectrometer. Trace elements such as: Al, Li, Sb, As, U, Th and I were analyzed by ICP-MS (Finnigan Mat Sola). Anions: Cl^-, SO_4^{2-}, Br^-, NO_3^-, NO_2^- and PO_4^{3-} were determined by ion chromatography (Dionex DX-4500i).

3.2 Physical parameters

The ***water content*** is defined as the ratio between the weight of the water lost after heating the sample to 110 °C for 24 hours and the weight of the dried material, expressed as percentage.

The ***porosity*** or ***water adsorption*** was measured by the hydrostatic balance method, (Norm ISO 6783-1982 or DIN 52103). The water porosity is defined as the ratio between the weight of the water gained after saturating the sample by submergence in water and the weight of the dried clay, expressed as percentage.

The ***density*** of the gouge fragment was measured by the pycnometer method and it is defined as the weight in the volume unit of a considered substance. In order to determine the occupied volume by a substance, whose dried weight is known with precision, the removed water weight by that substance is used.

3.3 Physico-chemical parameters

The physico-chemical parameters determined are: soluble salts, exchangeable cations and cation exchange capacity (CEC).

Soluble salts have been analyzed in an aqueous extract solution, as described in section 3.1.4.

Exchangeable cations were determined by the Chapman displacement method by means of successive washing with ammonium chloride 1M in a 60% ethanol/water solution, at pH=8.5 and after washing the soluble salts with a 60% ethanol/water solution (at 1:5 solid to liquid ratio with crushed rock samples sieved at < 63 μm) to avoid dissolution of carbonates (Thomas, 1982).

For the **CEC** determinations, CIEMAT´s quality control procedure IMA/X8/BI-Q6 was used. The exchange sites of the sample (< 63 μm) are saturated in sodium by means of successive washing with sodium chloride 1M. The adsorbed sodium is displaced by successive extractions with ammonium chloride 1M in a 60% alcohol/water solution at pH = 8.5. (Rhoades, 1982).

3.4 Isotope Analyses

3.4.1 Stable isotopes (^{13}C, ^{18}O)

Stable isotopes (^{18}O, ^{13}C) in calcite macrocrystals scraped from coatings was determined by mass spectrometer in Consejo Superior de Investigaciones Científicas of Granada. Calcite samples reacted with ultrapure phosphoric acid at 25°C, according to the McCrea reaction (1950):

$$2PO_4H_3 + 3CO_3Ca \Leftrightarrow (PO_4)2Ca_3 + 3H_2O + 3CO_2$$

The CO_2 obtained is introduced in a mass spectrometer for its isotope analysis, once it has been separated from the rest of the secondary products and purified by means of a system of cold traps at a vacuum of 10^{-4} mm Hg.

3.4.2. Radioactive isotopes

U series disequilibrium was determined at CIEMAT by alpha-spectrometry, according to the following procedures: "Procedure for the determination of U isotopes in soils by alpha spectrometry" (PR-X2-09) and "Procedure for the determination of ^{230}Th in soils" (PR-X2-01). ^{226}Ra was determined by gamma spectrometry.

4 Chemical composition

The chemical composition of major and minor elements was determined on gouge materials only, since there was not enough sample mass from coatings (Table 4- 1 and Table 4- 2).

Total CO_2 corresponds to inorganic CO_2, since organic C is negligible. Sample KI0025F03/51.9 m presents the highest CO_2 content, due to the fact that calcite is among the essential minerals.

High CaO contents are observed in KI0025F03 at 63.2 m and 73.1 m. Calcite is not responsible for this high content, since it is absent in both samples, as shown in Table 5-2. From a petrographic aspect, both samples present fine-grained bands rich in epidote and chlorite, which irregularly alternate with coarser-grained bands mainly constituted by quartz and plagioclase. Epidotes are reported to have 22-23% CaO (Deer et al, 1962). Though epidotization is a general process, it is stronger in these samples, and consequently, the CaO content is higher than in the other samples, where this epidote-rich banding is not as evident. This is in agreement with Elliasson´s (1993) assumption that part of the 20% loss of Ca in Äspö granite has been reprecipitated in fracture fillings as calcite, epidote and prehnite.

Fe oxi-hydroxides are not frequent, except in KI0025F03/ 63.2 m in which the high amount of Fe(III) can be explained by the increase of the amount of Fe oxi-hydroxides observed by SEM.

The samples are rich in Ba and Sr. Barite crystals are common. Tullborg et al (1999) have studied a fracture at 200 m depth in borehole KAS02 situated in Äspö Hard Rock Laboratory. They have separated feldspars and biotite from the adjacent wall rock. According to the chemical analyses of the feldspars, they contain high amounts of Sr (average: 880 ppm) and Ba (average: 2000 ppm), which are approximately in the same order of magnitude as our Sr (Average: 1294 ppm) and Ba (Average: 1054 ppm) data. Likewise, epidote in epidote-rich samples at Äspö contains in the order of 2000-4000 ppm of Sr. Consequently, the presence of barite may explain the high amounts of Ba whereas epidote and feldspars (especially plagioclase) may account for the high contents of Sr.

The presence of zircon and sphalerite can account for the Zr and Zn contents, respectively. U is in the range expected for these types of rocks. W can be accounted for by the presence of tungstite in some samples, and Cr by cromite.

Table 4- 1 Chemical composition of gouge fragments. Major elements (%)

	F03-51.9 m	F03-63.2 m	F03-73.1 m	F03-87.9 m	25F-88.8 m	KA2563A-154m (1)	KA2563A-154m (2)
SiO_2	55.08	45.86	59.19	58.22	58.98	61.15	60.16
Al_2O_3	16.60	17.50	16.40	18.10	17.70	15.90	14.80
CaO	6.20	9.30	10.10	2.60	4.20	4.70	4.30
Fe_2O_3	2.18	9.38	2.90	4.49	0.65	3.21	-
FeO	2.00	2.90	3.60	1.00	4.00	2.60	No sample
MgO	1.90	6.00	0.68	2.70	2.30	2.20	2.10
MnO	0.09	0.24	0.11	0.09	0.09	0.11	0.11
P_2O_5	0.96	1.10	0.74	1.20	1.10	1.00	1.20
Na_2O	3.90	1.40	2.70	5.20	5.20	3.20	3.10
K_2O	3.04	0.67	1.01	2.50	2.11	2.68	2.87
TiO_2	0.69	0.81	0.52	0.85	0.83	0.90	0.89
$CO_{2\ total}$	2.66	0.63	1.08	0.55	0.37	0.74	1.77
SO_2	0.08	0.10	0.32	0.08	0.24	0.18	0.20
H_2O^-	0.00	1.2	0.00	0.00	0.4	0.20	0.20
H_2O^+	1.46	0.84	0.60	1.87	1.67	1.18	0.04
SUBTOTAL	96.84	97.93	99.95	99.65	99.77	99.95	91.73
F≡O	0.06	0.08	0.02	0.02	0.05	0.05	0.05
TOTAL	96.78	97.85	99.93	99.63	99.72	99.90	91.68

(1) ground gouge; **(2):** natural loose gouge; * $Fe_2O_3 = Fe_2O_3$total - FeO · 1,1113; * F ≡ O is subtracted from SUBTOTAL; * SO_2 calculated from S total. * $H_2O^+ = H_2O_{\ total} - H_2O^- - CO_{2total} - SO_2$. Data base: results.xls; sheet:chem. anal. major

Table 4- 2 Chemical composition of gouge fragments. Minor elements (ppm)

	F03-51.9 m	**F03-63.2 m**	**F03-73.1 m**	**F03-87.9 m**	**25F-88.8 m**	**KA2563A-154m (1)**	**KA2563A-154m (2)**
As	<25	<25	<25	<25	<25	<25	<25
Ba	2000	320	535	1025	1075	1150	1275
Be	<5	<5	<5	<5	<5	<5	<5
Ce	94	270	125	110	130	160	160
Co	<5	24	<5	20	16	<5	20
Cr	51	59	25	45	27	38	85
Cs	0.8	0.7	<0.5	1.2	1.1	1.4	2
La	46	125	67	49	61	78	74
Li	14	51	10	34	29	27	23
Ni	18	45	<5	19	12	7.8	31
Rb	109	33	42	93	89	107	125
U	3.1	2.2	4.4	5.3	2.8	4	3.3
Sr	985	2375	1975	840	1125	955	805
V	67	145	155	80	73	90	89
W	<25	35	<25	<25	<25	<25	280
Y	19	59	21	24	23	31	32
Zn	85	175	25	87	73	80	140
Zr	115	110	73	140	130	160	310

(1): ground gouge; (2) natural loose gouge. Data base: results.xls; sheet: chem anal minor

5 Mineralogical composition and petrographic studies

5.1 Mineralogical composition

Gouge/coating pairs were analyzed by XRD quantitative analyses of the bulk sample, except in KI0025F02 where there was no gouge, and KA2563A, where there was no coating (Figure 5-1 to Figure 5-7). For the latter, determinations were performed in natural gouge (<0.063mm) and ground gouge from > 1 mm fragments. In all the X-ray patterns, mica stands for illite + sericite.

The content of each mineral is calculated according to the equation:

$$\%X_i = \frac{AX_i / \Pr X_i}{\sum AX / \Pr X} * 100$$

Where AX_i is the area of a specific peak calculated by multiplying the peak width by peak intensity; $\Pr X_i$ is the reference intensity ratio (RIR) of the mineral being determined.

The RIR (Schultz, 1964) used in the calculations are shown in Table 5- 1.

There has been some uncertainty with respect to peak at 4.04Å, since it can be either due to cristobalite or to plagioclase. SEM analyses, made on thin sections, confirmed that it was Na-Ca plagioclase.

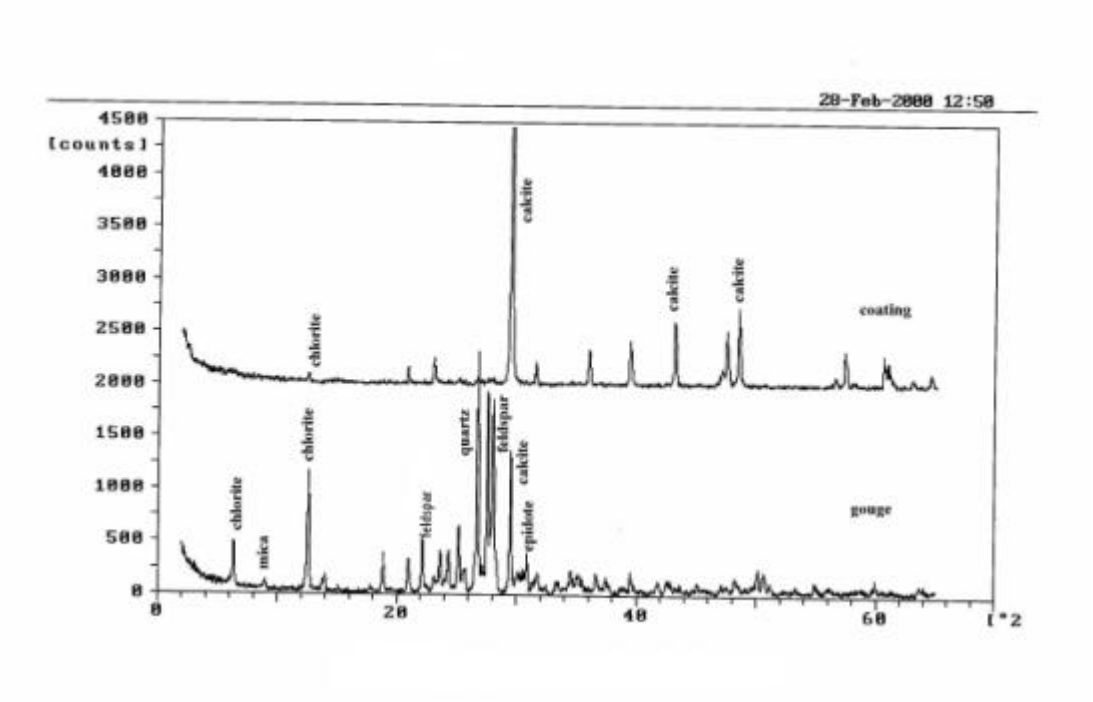

Figure 5-1 *XRD, borehole KI0025F03/51.9 m/# 6*

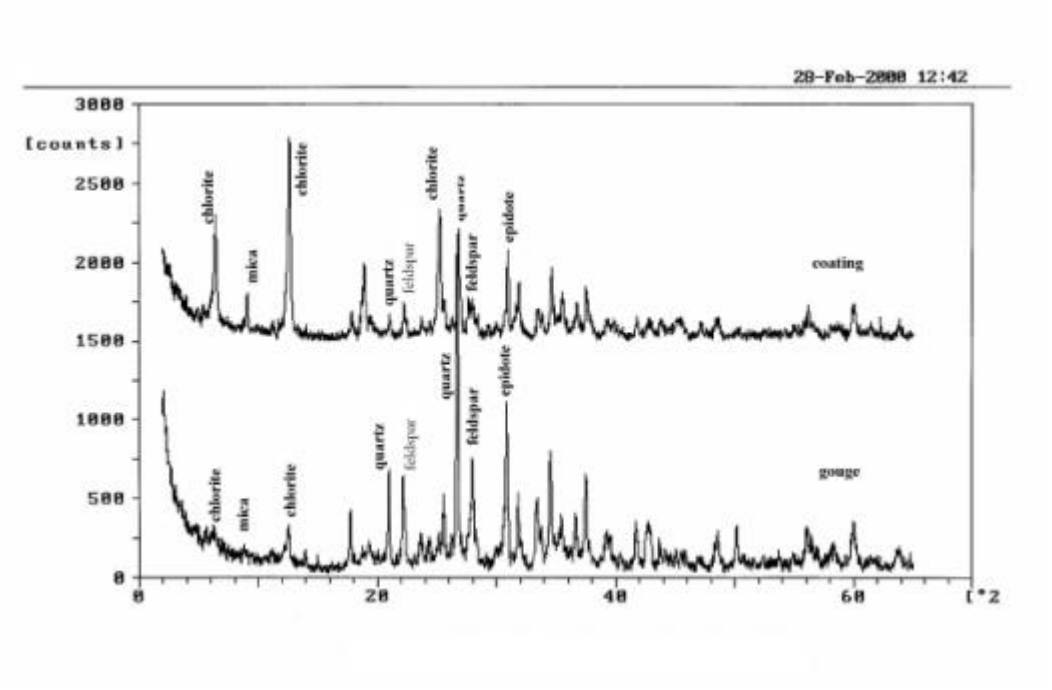

Figure 5-2 *XRD, borehole KI0025F03/63.2 m/# 22*

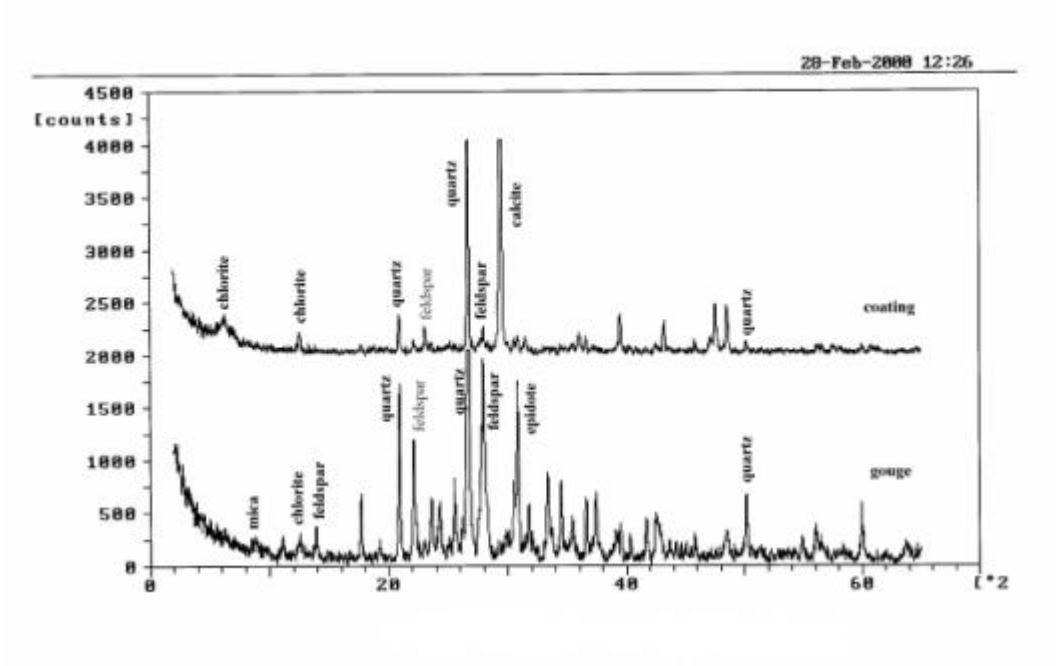

Figure 5-3 *XRD, borehole KI0025F03/73.1 m/# 20*

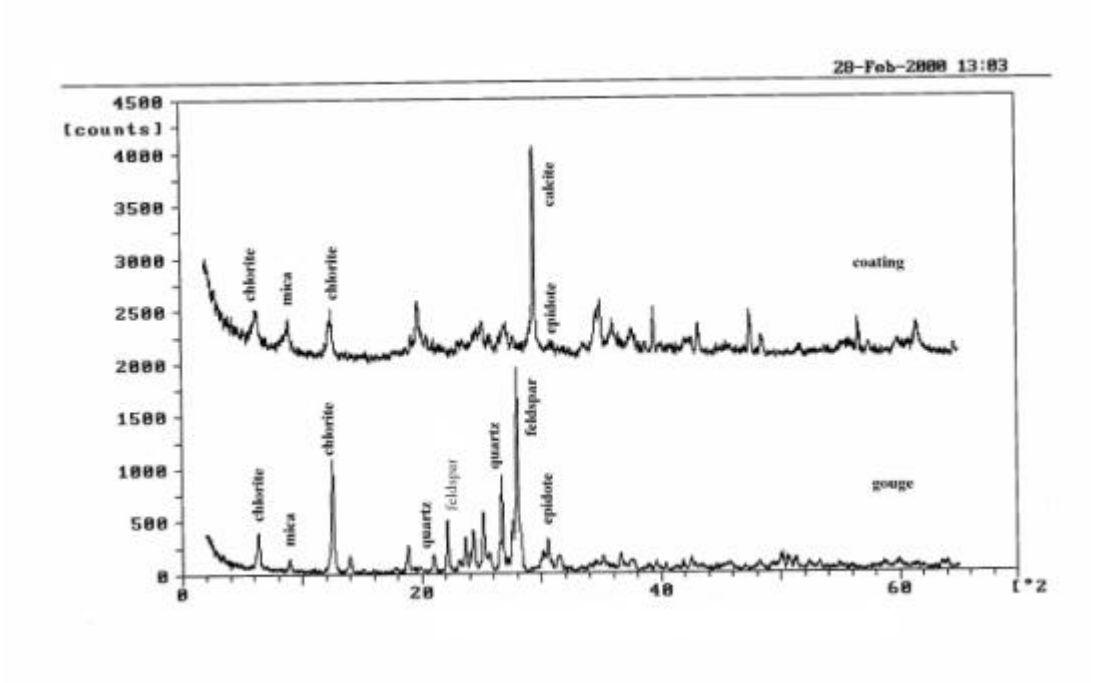

Figure 5-4 *XRD, borehole KI0025F03/87.9 m/# 13*

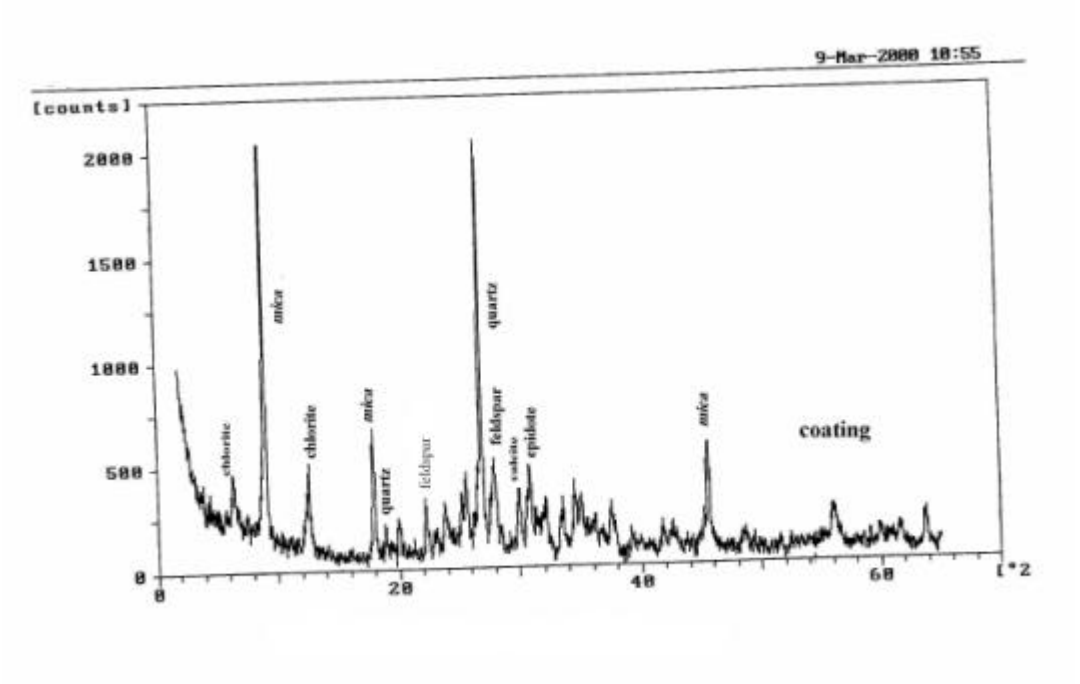

Figure 5-5 *XRD, borehole KI0025F02/ 93.9 m/ # 13*

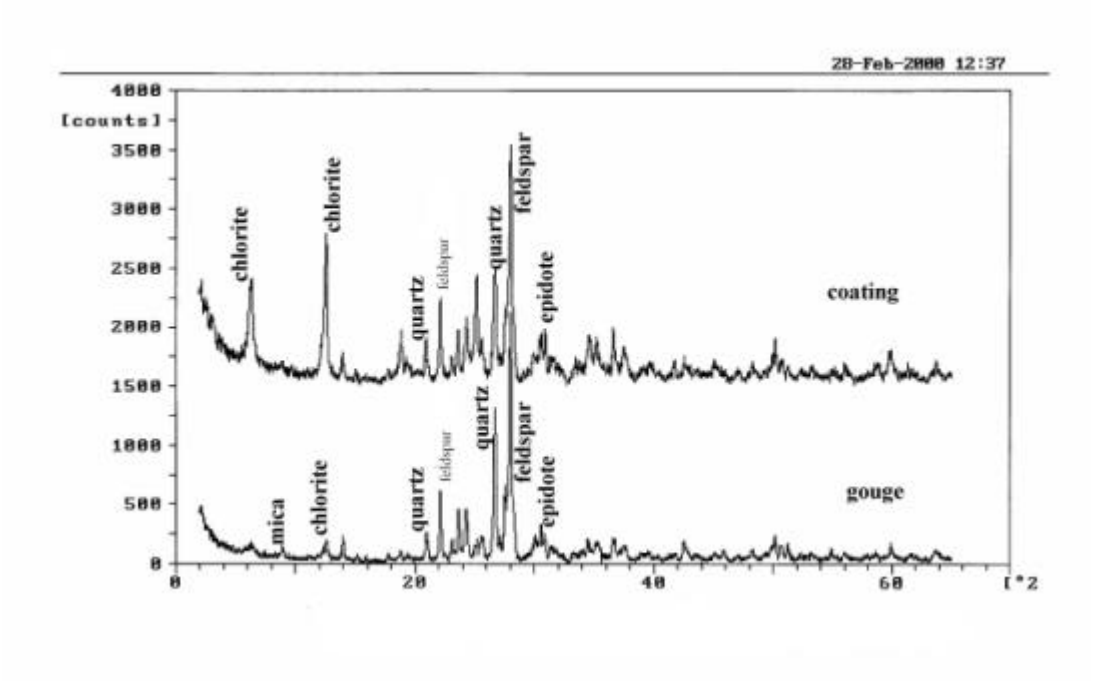

Figure 5-6 *XRD, borehole KI0025F/ 88.8 m/ # 22*

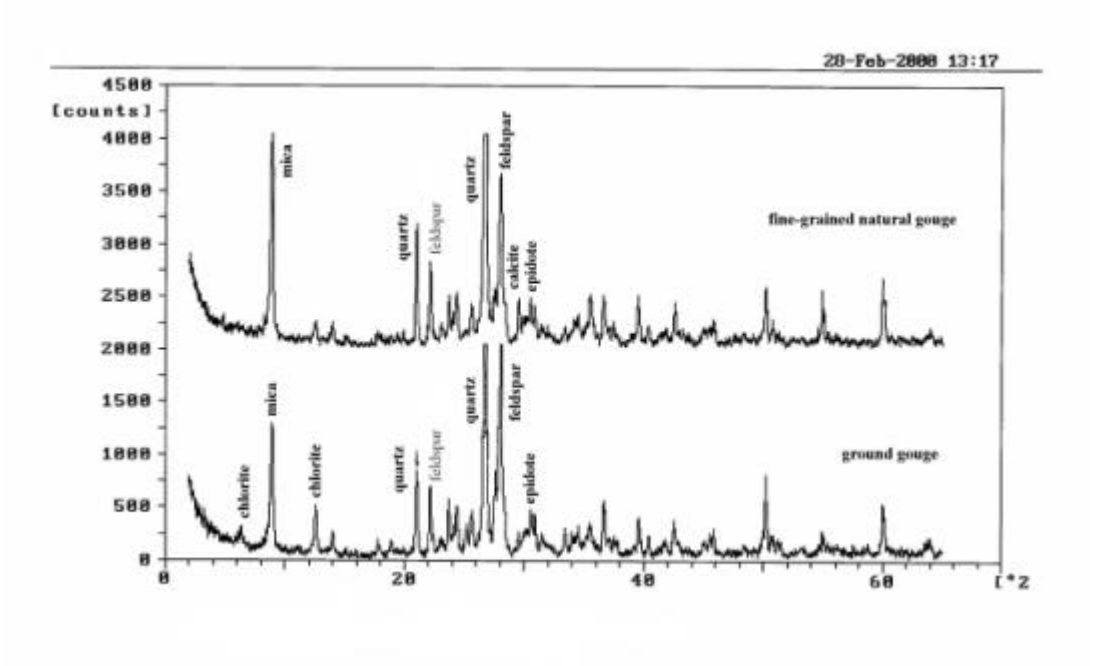

Figure 5-7 *XRD, borehole KA2563A/ 154 m/ # 6*

Table 5- 1 Reference intensity ratio (RIR)

Mineral	RIR
Phyllosilicates	0.10
Quartz	1.45
Feldspars (K-feldspars + plagioclase)	1.00
Calcite	1.00
Epidote	0.90

Table 5-2 shows the semiquantitative mineralogical composition obtained by XRD.

Gouge material are mainly formed by phyllosilicates (chlorite and illite), recrystallized quartz, feldspars (plagioclase and K-feldspar) and epidote. On the other hand, coatings are fundamentally composed of phyllosilicates and calcites and, in less proportion, quartz. Feldspars and epidote, present in coatings, most probably were scraped off from the wall rock together with the coatings.

Oriented aggregates were done in coatings from KI0025F03 (87.9 m, # 13)¸ KI0025F (88.8 m, #22) and ground gouge from KA2563A (154 m, # 6), to confirm the presence of smectite, which was doubtfully observed by SEM in the last two boreholes. These aggregates were treated with ethylene-glycol and the XRD confirmed the presence of smectite in the coating corresponding to KI0025F03 (87.9 m, # 13)¸ and the absence of this clay mineral in the other two boreholes (Figure 5-8).

Table 5-2 Semiquantitative composition (XRD) (%)

BOREHOLE/DEPTH (m) /STRUCTURE ID/MATERIAL	QUARTZ	K-FELDSPAR + PLAGIOCLASE	EPIDOTE	CALCITE	PHYLLOSILICATES		TOTAL
					CHLORITE *	MICA(illite) *	
KI0025F03/51.9/#6 / GOUGE	15	30	5	15	30	5	100
KI0025F03/51.9/#6 /COATING	Traces	Traces	-	98	traces	Traces	98
KI0025F03/63.2/#22 / GOUGE	55	10	10	-	20	5	100
KI0025F03/63.2/#22 /COATING	10	5	10	-	60	15	100
KI0025F03/73.1/#20 /GOUGE	15	45	20	-	15	5	100
KI0025F03/73.1/#20 /COATING**	30	10	5	50	5	Traces	100
KI0025F03/87.9/#13 /GOUGE	10	35	5	-	40	10	100
KI0025F03/87.9/#13 /COATING	5	10	5	25	30	25	100
KI0025F02/93.9/#13 /COATING	25	20	10	10	5	30	100
KI0025F/88.8/#22 / GOUGE	20	65	10	-	5	traces	100
KI0025F/88.8/#22 / COATING	10	45	10	Traces	30	5	100
KA2563A/154/#6 / GROUND GOUGE (<0.063mm)	40	40	5	-	5	10	100
KA2563A/154/#6 / NATURAL LOOSE GOUGE (<0.063 mm)	25	50	10	-	5	10	100

**chlorite and mica are calculated from the total % of phyllosilicates.*

*** Silica sample holder used due to the small amount of sample, the rest of samples measured with Al sample holder.*

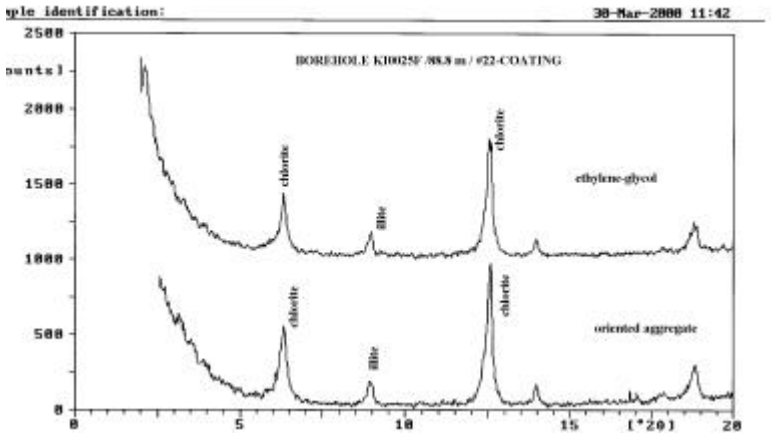

a

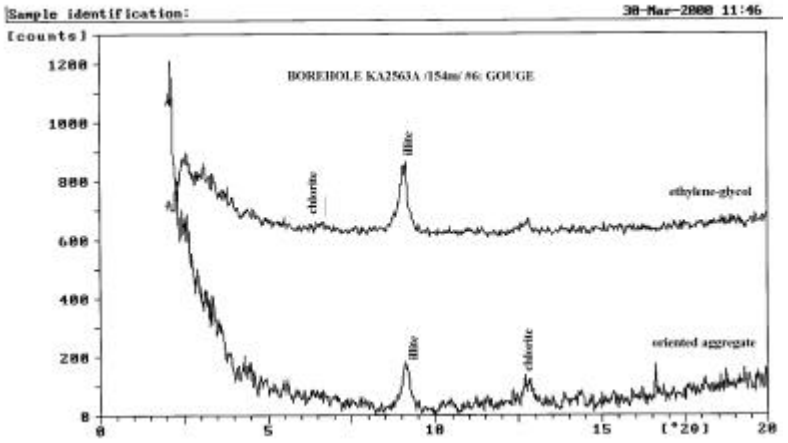

b

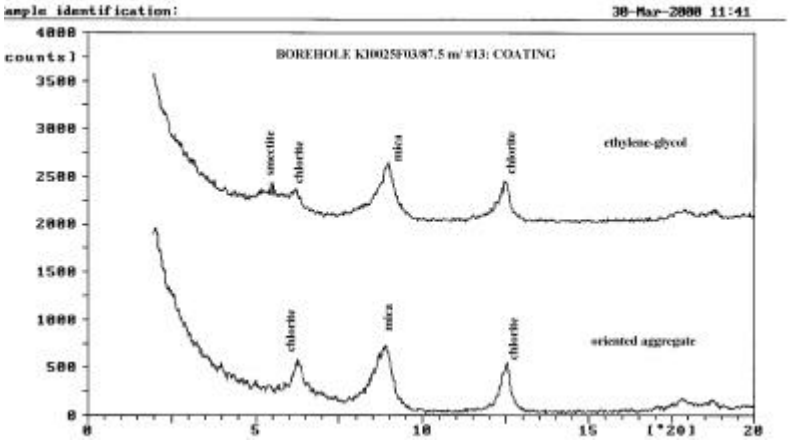

c

Figure 5-8 *XRD of oriented aggregates. Smectite was only confirmed in* **c**

5.2 Petrographic study

Thin sections of wall rock and the corresponding gouge fragments were studied by optical microscopy. The main object of the SEM determinations in gouge and coating splinters was to identify the trace and opaque minerals, as well as the clay minerals, since the <2μm fraction was not possible to separate due to lack of sufficient amount of sample. This study was made by comparing the mineralogical and petrographic characteristics of the rock, gouge material and coating of the same structure in the intersection point with the different boreholes.

5.2.1 Structure # 6

This structure intersects borehole KI0025F03 at 51.9 m and KA2563A at 157.2m. According to the March ´00 model, structure #7 intersects KA2563A at 153.4 m, which is the depth at which the sample was collected. However, the intersection points of both structures have been differently interpreted in previous models (Jan Hermanson´s written personal communication, 2000). In this work, we will follow J. Hermanson´s suggestion as to consider structure #6 as part of a network of conductive fractures with varying orientations and geology, in which structure #7 is also included. The mineralogical and petrographic comparison between both intersection points is shown in Table 5- 3 and the differences observed in Table 5- 4.

The intersection points of structure #6 show different characteristics. In KA2563A; 154 m fine-grained gouge material is abundant and it is essentially constituted by quartz and feldspars. Gouge fragments > 1mm are scarce and their composition is heterogeneous. Some of them show abundant plagioclase and feldspars, whereas others are mainly formed by epidote and chlorite.

In contrast KI0025F03; 51.9m does not have < 1mm gouge and there is no significant mineralogical or petrographic differences between the rock and the gouge fragments. Precipitation of calcite, both as coating and fissure and void fillings, is significant. The presence of fluorite indicates element mobility.

Fe oxi-hydroxides are present in both intersections, but in KA2563A they are associated with Cl, Ca and Si impurities which are probably residues due to evaporation of groundwaters (Säfvestad, A et al, 1999).

Table 5- 3 Mineralogical and petrographic comparison of rock, gouge and coatings of structure # 6

KI0025F03 51.9m	KA2563A 154m
ROCK	
Äspö diorite (Annex B-Fig. 1 a) Essential minerals Moderately sericitized Na-Ca plagioclase; total chloritization of biotite (Annex B-Fig. 1 b); abundant epidote, also from alteration of biotite (Annex B-Fig. 1 a); lenticles of recrystallized quartz; sphene with alteration rims (Ti oxides) (Annex B-Fig. 1 c), calcite filling late fissures and voids. Accessory minerals: K-feldspars; opaques with carbonate rim; fluorite.	No rock sampled
GOUGE FRAGMENTS	
Similar to rock (Annex B-Fig. 1 e; Annex C-Fig- 1 a). Accessory minerals: barite, pyrite, zircon, Fe oxi-hydroxides, calcite in fissures (Annex B-Fig. 1 d), fluorite in voids.	Abundant loose gouge material <1mm. Fragments >1mm are very heterogeneous. Some are fundamentally formed by epidote and chlorite (from biotite) (Annex B-Fig. 2 a); others by quartz, K-feldspar and plagioclase; (Annex B-Fig. 2 b, c). Accessory minerals: barite, collophorm Fe oxi-hydroxides with Cl, Ca and Si impurities (Annex C-Fig. 1 b), zircon, pyrite.
COATING	
Calcite coats the fracture surface	No coating

Table 5- 4 Mineralogical and petrographic differences in the intersection points of structure # 6

KI0025F03 51.9m	KA2563A 154m
GOUGE	
Gouge fragments >1mm but no loose natural <1mm material	Abundant <1mm gouge material with some >1mm heterogeneous gouge fragments .
Epidote- quartz-poor gouge	Epidote-quartz-rich gouge
Alteration of sphene to Ti oxides (probably anatase)	No sphene observed
Fe oxi-hydroxides without impurities	Fe oxi-hydroxides with Cl, Ca and Si impurities
COATING	
Calcite coating rock and filling fissures	Coatings not observed.

5.2.2 Structure # 13

This structure intersects borehole KI0025F03 at 87.9m and KI0025F02 at 93.9m. Coatings of both intersection points were studied by SEM due to the scarce amount of sample. Table 5- 5 shows the comparative study.

Tectonization seems to be stronger in KI0025F03 (87.9 m), producing fine-grained zones and abundance of clay minerals. Hydrothermal processes are represented by the presence of epidote (KI0025F02 ; 93.9 m) filling fissures in the rock.

The main differences found in the intersection points of #13 with boreholes KI0025F03; 87.9 m and KI0025F02 ; 93.9 m are shown in Table 5- 6.

Table 5- 5 Mineralogical and petrographic comparison of rock, gouge and coatings of structure #13

KI0025F03 87.9m	KI0025F02 93.9m
ROCK	
Tectonized zone intersected by fine-gained granite. Cataclastic texture with fine-grained irregular bands (Annex B-Fig. 3 a). Essential minerals: Na-Ca plagioclase: moderately sericitized, biotite altered to chlorite (Annex B-Fig. 3 b) and muscovite, epidote, quartz. Accessory minerals: fluorite filling late fissures; opaques with and without carbonate rims (Annex B-Fig. 3 c); K-feldspars, sphene altered to anatase, zircon, apatite.	Medium-grained mylonite (Annex B-Fig. 4 a). Essential minerals: Abundant quartz and K-Feldspar. Plagioclase moderately sericitized, scarce chlorite (from biotite) and epidote. Muscovite from biotite. Epidote filling fissure. Accessory minerals: Fe oxides (cleavage planes of former biotite, alteration of opaques, surrounding grains); opaques with/without carbonate halo; apatite; fluorite and calcite in voids (Annex B-Fig. 4 b).
GOUGE FRAGMENTS	
Very similar to rock, with coarser grains and less developed fine-grained bands. Na-Ca plagioclases more sericitized (Annex B-Fig. 3 d). Accessory minerals: fluorite in voids, apatite, calcite, zircon, titanite (from sphene), pyrite, galena, sphalerite, molibdenite, Fe oxi-hydroxides with Si, Ca, Cl, Al, Mg impurities in close association with Fe-Mn oxi-hydroxides; saponite and smectite .	No gouge
COATING	
Saponite, transition from chlorite to saponite (Annex C-Fig. 2, 3); calcite impregnating saponite and chlorite, cromite, zircon, pyrite (Annex C-Fig. 5 a, b), galena, Fe oxi-hydroxides without impurities, illite (Annex C-Fig. 4). Minerals from the rock: chlorite (from biotite), orthose, Na-Ca plagioclase, epidote, quartz.	Minerals from rock: Na-Ca plagioclase partially transformed into albite, biotite altered to chlorite and muscovite, K feldspars, quartz, epidote, sphene. Zircon, calcite, apatite, pyrite, sphalerite, tungstite (Fe-poor wolframite?), Fe oxi-hydroxides, U oxide within silicates. Abundant illite (Table 5-2). Graphite (?) as thin coating on K-feldspar. (Annex C-Fig. 6 a-f).

Table 5- 6 Mineralogical and petrographic differences in the intersection points of structure #13

KI0025F03; 87.9 m	KI0025F02 ; 93.9 m
ROCK	
Scarce quartz, plagioclase and K-feldspar	Abundant quartz, plagioclase and K-feldspar
Abundant chlorite, epidote, phyllosilicates (sericite, illite)	Scarce chlorite, epidote, phyllosilicates
Fine-grained bands	Coarse-medium size grains, bands less apparent
Fe oxi-hydroxides not observed	Fe oxi-hydroxides: in fissures, intergranular positions
No muscovitization	Biotite altered to muscovite
Sericitization of plagioclase and K felspars	Plagioclase and K-feldspars better preserved
Epidote not in fissures	Epidote filling fissures
GOUGE	
Variety of sulphur minerals: pyrite, galena, sphalerite.	No gouge
Opaques with carbonate rims.	
Fe oxi-hidroxides with and without Si, Ca, Cl	
Probable saponite	
COATING	
Saponite (chlorite →transition zone → saponite)	Saponite not observed
U not found	Traces of U oxide (associated with silicates)
No tungstite, graphite (?)	Tungstite and graphite (?) observed
Presence of cromite and sericite (illite)	No cromite, illite

5.2.3 Structure # 22

This fracture intersects boreholes KI0025F03 at 63.2 m and KI0025F at 88.8 m (Table 5- 7). The differences between these two intersection zones are represented in Table 5- 8.

Structure #22 intersects mylonitized Äspö diorite with cataclastic texture. Fine-grained bands are mainly formed by epidote and chlorite, both coming from alteration of biotite. The rock in KI0025F presents a stronger sericitization of plagioclase than KI0025F03.

Gouge material is texturally and mineralogically similar to the rock in both boreholes. The variety of sulphides in KI0025F is not observed in KI0025F03.

With respect to coatings, both intersection points present clay-rich coatings, (75% in KI0025F03 and 35% in KI0025F, Table 5-2), comprising chlorite, fundamentally, and illite.

Table 5- 7 Mineralogical and petrographic comparison of rock, gouge and coatings of structure #22

KI0025F03 63.2m	KI0025F 88.8 m
ROCK	
Mylonitized Äspö diorite. Fine grained bands (epidote, chlorite) irregularly alternating with coarser-grained bands (quartz, plagioclase). (Annex B-Fig. 5 a) Essential minerals: slightly sericitized plagioclase, biotite altered to chlorite, epidote, quartz. Accessory minerals: fluorite filling voids; calcite filling fissures and voids; opaques with carbonate rims (Annex B-Fig. 5 b); K-feldspars, macrocrystalline sphene altered to anatase, zircon.	Mylonite. Cataclastic texture (Annex B-Fig. 6 a) with formation of kinks in chlorite from alteration of biotite. Fine-grained bands formed by epidote irregularly alternating with coarser-grained bands. Essential minerals: Macrocrystals of strongly sericitized plagioclase, chlorite from biotite, recrystallized quartz, epidote, fissural chlorite. Accessory minerals: K-feldspar, sphene altered to anatase, fluorite, calcite in voids, opaques, zircon.
GOUGE FRAGMENTS	
Fine-grained bands formed by epidote and chlorite, fundamentally. Biotite altered to chlorite and epidote (Annex B-Fig. 4 c). Accessory minerals: slightly altered plagioclase, K-Feldspar, quartz, fluorite in voids, apatite, zircon, pyrite, Fe oxi-hydroxides.	Similar to rock, though plagioclase somewhat more altered. Strong deformation (Annex B-Fig. 6 c) Essential minerals: Very strongly sericitized Na-Ca plagioclase and albite (from Na-Ca plagioclase), quartz (Annex B-Fig. 6 b), epidote, sphene broken macrocrystals with chlorite filling fissures and voids within the crystal. Accessory minerals: calcite in voids, zircon, K-feldspar, pyrite, sphalerite, chalcopyrite, apatite, tungstite, Fe oxi-hydroxides with Ca, Cl, Si impurities (Annex C-Fig. 7 b-f).
COATING	
Studied only by XRD: Table 5-2 Presents the highest contents of chlorite (60%) of all the samples. Quartz, plagioclase + K-feldspars and epidote are scarce.	SEM: splinter and scraped off material Essential minerals: biotite to chlorite, K-feldspar, albite and Na-Ca plagioclasse, epidote, calcite, quartz, sphene altered to anatase. Accessory minerals: Fe oxi-hydroxides, apatite, barite, galena, pyrite, zircon, cromite (Annex C-Fig. 7 a), tungstite. Graphite coating grains?

Table 5- 8 Mineralogical and petrographic differences in the intersection points of structure #22

KI0025F03 63.2m	KI0025F 88.8 m
ROCK	
Less sericitization of plagioclase	Plagioclase strongly sericitized
Less chloritization of biotite	Biotite strongly altered to chlorite, epidote
GOUGE	
Only pyrite observed	Variety of sulphide minerals: pyrite, sphalerite, chalcopyrite.
No tungstite	Tungstite present
Fe oxi-hydroxides without impurities	Fe oxi-hydroxides with Ca, Cl, Si impurities
Abundant phyllosilicates	Less phyllosilicates (XRD)
COATING	
Abundant phyllosilicates (XRD)	Less phyllosilicates (XRD)
Not observed	Galena, pyrite

5.2.4 Structure # 20

This feature intersects KI0025F03 at 73.1 m and has not been identified in any other sample studied in this work (Table 5- 9).

This intersection is similar to the other structures from a mineralogical and textural point of view. The coating is poor in phyllosilicates, in contrast to the gouge material.

Table 5- 9 Petrographic study of structure #20 in KI0025F03 at 73.1 m

ROCK
Mylonite forming fine-grained bands (epidote) alternating with coarser-grained bands (quartz, plagioclase) (Annex B-Fig.7 a). Essential minerals: Epidote, strongly sericitized plagioclase (Annex B-Fig. 7 b), recrystallized quartz, chlorite from alteration of biotite; opaques. Accessory minerals: zircon, calcite filling voids in coarser-grained bands, Fe oxi-hydroxides.
GOUGE
Similar to rock in texture and minerals Essential minerals: Plagioclase somewhat less sericitized than in rock (Annex B-Fig. 7 c), epidote (Annex C-Fig. 8 d), lenticles of recrystallized quartz, sphene with alteration rims (Ti oxides), biotite altered to chlorite. Rich in phyllosilicates. Accessory minerals: pyrite, fluorite (Annex C-Fig. 8 a), zircon, apatite, barite, calcite, Fe oxi-hydroxides with Si, Ca and Cl impurities (Annex C-Fig. 8 c). Probable remobilization of zircon (Annex C-Fig. 8 b)
COATINGS
Not studied by SEM because of lack of sample. Significantly less phyllosilicates (chlorite and illite) than gouge (Table 5-2).

5.3 Discussion of results

The different structures intersect highly deformed rocks. The amount of gouge material varies, and they are, in general, texturally and mineralogically similar to the host rock. Gouge material may be heterogeneous within the fragments of the same sample. This material fundamentally comprised > 1 mm fragments, except in KA2563A; 154 m, in which a significant amount of the gouge material was formed by natural fine-grained unconsolidated material (< 1mm, Table 2- 3). This fine-grained gouge is mainly constituted by quartz, and plagioclases (Table 5-2).

The only clay minerals present in significant amounts are chlorite and illite. Traces of swelling clays (saponite) are identified in coatings from KI0025F03 at 87.9 m, where a transition from chlorite to saponite can be seen, indicating a gradual loss of Fe and increase of Mg (Annex C-Fig. 2 a, b).

Na-Ca plagioclases and albite (probably from alteration of the former) are sericitized in different degrees and biotite is totally altered to idiomorphic-subidiomorphic epidote (Tullborg, 1999 b) and chlorite, that still bear remnants of heavy minerals from biotite along the cleavage planes.

Fe oxi-hydroxides usually exhibit a carbonate halo (calcite) (Annex B-Fig. 3 c and 5 b) and present Cl, Ca and Si impurities, due to the evaporation of Cl-Ca-rich groundwaters, which are present in the zone.

Calcite occurs in voids and fissures or overlying the rest of the minerals in coatings (Annex A, Fig. 2, 4, 6, 8) It is preferentially observed in coatings, whereas in rocks and gouge fragments it occurs as an accessory mineral. According to textural relationships only, calcite, in these samples, seems to be a recent mineral: calcite-filled fissures cut across the rest of the minerals (Annex B, Fig. 1d), and macrocrystals are observed to be precipitated on top of the fracture surface. However, the existence of several generations of calcite is not ruled out, as fracture calcites have been used as paleohydrological indicators, due to their formation, dissolution or recrystallization during all the time that the fractures have been hydraulically active (Stanfors et al, 1999).

Fluorite is quite frequent and fills voids, both in the rock and gouge fragments and another generation of epidote has been observed filling a fracture in mylonite from KI0025F02 (93.9 m). Fluorite and epidote indicate hydrothermal processes.

6 Isotope studies

6.1 Stable isotopes

$\delta^{13}C$ and $\delta^{18}O$ were determined on four samples of calcite from fracture fillings and gouge (Table 6- 1). The calcite corresponding to sample from 51.9 m in KI0025F03 named "calcite in rock" was found filling a fissure that was opened when the rock was being cut for thin section.

Table 6- 1 Isotopic signature of calcites from fracture fillings and gouge

SAMPLE	$d^{13}C_{(PDB)}$ ‰	$d^{18}O_{(PDB)}$ ‰
KI0025F03; 51,9m. # 6 CALCITE COATING	-14,1	-11,6
KI0025F03; 51,9m. # 6 CALCITE IN ROCK	-9,4	-12,4
KI0025F03; 73,1 m. # 20 CALCITE MACROCRYSTAL IN COATING	-11,1	-14,1
KI0025F; 88,8m. # 22 CALCITE IN GOUGE	-11,3	-6,5

The $\delta^{13}C$ signatures vary from -9.4 to -14.1 ‰ and $\delta^{18}O$ from -6.5 to -14.1 ‰, relative to PDB. These values indicate, in general, a moderate enrichment of ^{13}C and rather low values of ^{18}O.

The large variations in the stable isotope composition of calcites from a limited area of a single fracture plane indicate water-rock interactions during periods with different types of groundwaters. According to Tullborg et al (1999 a), groundwater in the Äspö tunnel passing under the Baltic Sea, as well as sediment porewater are significantly modified by sulphate-reducing bacteria. Sulphate reduction is taking place at present in brackish water with ^{18}O values of -6 to -8 ‰. Consequently, most of the calcites sampled at Äspö (with $\delta^{18}O$ values between 0.0 to -17.0 ‰), despite their large variations in $\delta^{18}O$ values, may have a low temperature origin, since sulphate-reducing bacteria cannot be productive at high temperatures.

The ^{13}C values in this work suggest that the C source of these calcites could be a mixture of edaphic and atmospheric CO_2 (Reyes et al, 2000; Wallin et al, 1999). According to the ^{18}O values and to the presence of sulphate-bearing bacteria, these calcites are probably precipitated at ambient temperature from a mixture of meteoric and glacial water. However, a hydrothermal origin should not be ruled out. As Wallin and Peterman (1999) point out for the Laxemar area "some of the carbonates with higher $\delta^{13}C$ values may also be a result of dissolution of old hydrothermal carbonates and reprecipitated with a hydrothermal signature left in the C sources". Similar results were obtained for calcite fracture filling in drillcores at Äspö (Tullborg and Wallin, 1991).

6.2 Radioactive isotopes

The radioactive isotopes analyzed are ^{238}U, ^{234}U, ^{230} Th and ^{226} Ra (Table 6- 2). ^{230}Th could not be determined in KI0025F03 (51.9 m) and KA2563A (157 m) due to lack of sample.

The $^{234}U/^{238}U$ activity ratio (AR) is approximately 1, except in KI0025F03 (63.2 m) in which it is less than 1. This implies that ^{234}U is in equilibrium with ^{238}U in the former case. Consequently, there has been neither leaching nor precipitation of U for at least the last 1,7 My in most of the samples. However, in KI0025F03 (63.2 m) a slow leaching of ^{234}U is assumed since $^{230}Th/^{234}U$ is considered in equilibrium, which indicates that ^{230}Th is supported by ^{234}U.

In KI0025F03 at 73.1 m and 87.9 m and KI0025F at 88.8 m the activity ratio of $^{230}Th/\ ^{234}U$ and $^{230}Th/^{238}U$ is less than unity, indicating a recent uptake of U in equilibrium since ^{230}Th is considered to be immobile.

In general, there is an accumulation of ^{226}Ra, except in KI0025F03 at 73.1 m. The highest ratios are present in structure #22, and it could be related to the presence of Ba as barite.

Table 6- 2 Radioactive isotopes

borehole/depth (m)/ structure	isotope	activity (Bq/K)	uncertainty	234U/238U	230Th/234U	230Th/238U	226Ra/230Th
KI0025F03/51,9 /# 6	**U-238**	4,858E+01	2,759E+00	1,003			
	U-234	4,873E+01	2,764E+00				
	Ra-226	bdl					
KI0025F03/63,2 /# 22	**U-238**	2,854E+01	4,199E+00				
	U-234	2,565E+01	3,944E+00	0,899	0,975	0,876	7,188
	Th-230	2,500E+01	3,400E+00				
	Ra-226	1,797E+02	6,086E+01				
KI0025F03/73,1 / #20	**U-238**	6,490E+01	3,390E+00				
	U-234	6,360E+01	3,350E+00	0,980	0,755	0,740	0,768
	Th-230	4,800E+01	3,400E+00				
	Ra-226	3,684E+01	3,033E+01				
KI0025F03/87,9 /# 13	**U-238**	6,312E+01	3,324E+00				
	U-234	6,435E+01	3,367E+00	1,019	0,901	0,919	2,278
	Th-230	5,800E+01	3,500E+00				
	Ra-226	1,321E+02	4,752E+02				
KI0025F/88,8 / # 22	**U-238**	3,717E+01	4,913E+00				
	U-234	3,915E+01	5,071E+00	1,053	0,817	0,861	3,897
	Th-230	3,200E+01	2,400E+00				
	Ra-226	1,247E+02	4,877E+01				
KA2563A/154/ # 6 ground gouge, <0,063 mm	**U-238**	4,568E+01	2,647E+00	1,014			
	U-234	4,630E+01	2,669E+00				
	226Ra	1,21E+02	5,38E+01				
KA2563A/154/#6 natural gouge, <0,063 mm	**U-238**	4,17E+01	2,56E+00	1,096			
	U-234	4,57E+01	2,71E+00				
	Ra-226	bdl					

bdl: below detection limit

7 Physico-chemical parameters

Given that the tracer retention depends on the pore structure and surface mineralogy of the fractures and of the rock matrix adjacent to the conductive structures, the determination of some physical parameters and the cation exchange capacity has been carried out. The analyzed samples correspond to gouge material obtained from different boreholes which intersect structures # 6, # 13, # 20 and # 22 .

The physical parameters determined in the rock samples are density and water adsorption, which, in turn, were used to calculate the porosity (Table 7- 1).

The water adsorption measurements ranged from 0.26 to 0.78 %; the density of the samples varied from 2588 to 2891 Kg/m^3 and the calculated porosity from 0.71 to 2.05 % (volume). Figure 7- 1 shows that the correlation between the density of the gouge fragments and total Fe_2O_3 is not bad. This is supported by the presence of Fe-bearing minerals (Fe-oxihydroxides), which have higher densities.

Table 7- 1 Physical characteristics of the samples

Borehole	Depth (m)	Structure ID	Rock material	Density (Kg/m^3)	Water adsorption (%)	Porosity (n) [(1)] (%) volume
KI0025F03	**51.9**	# 6	ÄD	2588	0.42 ± 0.05	1.08
KI0025F03	**63.2**	# 22	Mylonite in diorite	2891	0.65 ± 0.08	1.84
KI0025F03	**73.1**	# 20	Mylonite	2765	0.26 ± 0.01	0.71
KI0025F03	**87.9**	# 13	Tectonized zone in ÄD with F-GG	2683	0.78 ± 0.01	2.05
KI0025F	**88.8**	# 22	Altered ÄD	2719	0.72 ± 0.02	1.92
KA2563A	**154**	# 6	Fine-grained gouge	2725	0.51 ± 0.04	1.37

ÄD: Äspö diorite; F-GG: fine-grained granite

(1) $n = \frac{r_s}{r_s + \frac{r_w}{w}} \times 100$, where ρ_s is the grain density, ρ_w is the water density and w is the water absorbed (m_{water}/m_{dry})

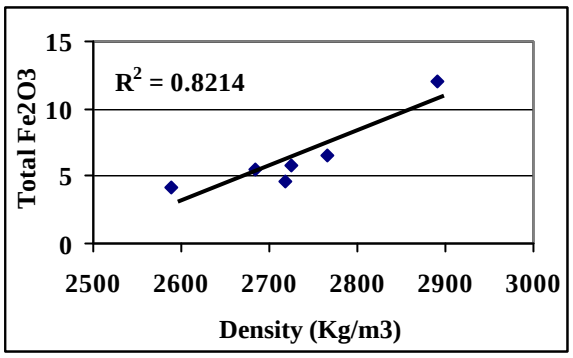

Figure 7- 1 *Correlation between Density and Total Fe_2O_3*

8 Cation Exchange Capacity (CEC)

In order to determine the cation exchange capacity of the rock samples, the possible soluble salts present in the samples were firstly analysed (Table 8- 1). The main ions present as soluble salts are Cl^-, SO_4^{2-}, HCO_3^-, Na^+, K^+ and Ca^{2+}, and in minor quantities, Mg^{2+}, Sr^{2+}, Ba^{2+}, Rb^+ and Cs^+. The pH of these solutions is highly alkaline, probably due to dissolution of carbonates. These ions can come from the redissolution of salts precipitated by evaporation of saturation waters and from the dissolution of some of the mineral components of the rock. The SEM mineralogical analyses have confirmed the existence of Ca and Cl impurities associated with Fe-oxihydroxides.

In order to avoid the dissolution of solid phases and to extract the cations which do not belong to the exchange positions, the soluble salts were washed with an alcohol solution (60% ethanol/water). The chemical composition of the leached solutions are shown in Table 8- 2. The results show that practically only Cl^-, Na^+ and K^+ were extracted.

Table 8- 1 Soluble salts obtained in the generic rock material from a distilled water solution at 1:10 solid to liquid ratio

Sample	KI0025F03	KI0025F03	KI0025F03	KI0025F03	KI0025F	KA2563A
Depth (m)	51.9	63.2	73.1	87.9	88.8	154
pH	9.0	8.9	8.9	7.9	9.0	8.5
Conductivity (µS/cm)	198	185	223	135	220	216
Br^- (mg/L)	n.d.	< 2	< 2	< 2	< 2	< 2
Cl^- (mg/L)	n.d.	7.5	14	12	16	31
SO_4^{2-} (mg/L)	n.d.	1.3	8.5	2.7	5.9	7.1
HCO_3^- (mg/L)	n.d.	84.1	99.2	53.2	75.2	81.2
Na^+ (mg/L)	14	13	24	16	21	15
K^+ (mg/L)	16.4	18	20	12	19	42
Ca^{2+} (mg/L)	15	3.0	9.0	5.0	5.6	5.5
Mg^{2+} (mg/L)	<2.0	7.0	1.9	<0.8	1.4	1.6
Sr^{2+} (µg/L)	195	28	75	54	58	52
Ba^{2+} (µg/L)	207	3.9	4.5	3.9	3.8	17
Cs^+ (µg/L)	0.3	<0.2	<0.2	0.74	0.51	0.48
Rb^+ (µg/L)	20	19	23	20	26	52
Li^+ (mg/L)	<0.01	0.04	<0.02	<0.02	<0.02	0.02
Al^{3+} (mg/L)	0.43	0.40	0.55	0.24	0.36	0.67
Fe^{3+} (mg/L)	<0.1	<0.06	<0.06	<0.06	<0.06	<0.06
Mn^{2+} (mg/L)	<0.1	<0.06	<0.06	<0.06	<0.06	<0.06
Zn^{2+} (mg/L)	<0.2	<0.1	<0.1	<0.1	0.15	<0.1

n.d.: not determined

Table 8- 2 Soluble salts obtained in the generic rock material from an alcoholic solution (60% ethanol/distilled water) at 1:5 solid to liquid ratio

Sample	KI0025F03	KI0025F03	KI0025F03	KI0025F03	KI0025F	KA2563A
Depth (m)	**51.9**	**63.2**	**73.1**	**87.9**	**88.8**	**154**
pH	8.57	8.55	8.39	8.55	8.21	8.42
Conductivity (μS/cm)	31.5	30.2	29.2	35.4	48.8	42.6
Br^- (mg/L)	< 1	< 1	< 1	< 1	< 1	< 1
Cl^- (mg/L)	18	16	15	16	17	20
SO_4^{2-} (mg/L)	0.3	< 0.1	0.9	0.26	1.9	1.5
HCO_3^- (mg/L)	n.d.	n.d.	n.d.	n.d.	n.d.	n.d.
Na^+ (mg/L)	14.0	17.0	16	19	27	20
K^+ (mg/L)	4.0	2.2	1.8	2.2	3.4	9.2
Ca^{2+} (mg/L)	< 4.0	< 4.0	< 4.0	< 4.0	< 4.0	< 4.0
Mg^{2+} (mg/L)	< 2.0	< 2.0	< 2.0	< 2.0	< 2.0	< 2.0
Sr^{2+} (mg/L)	< 0.1	< 0.1	< 0.1	< 0.1	< 0.1	< 0.1
Ba^{2+} (mg/L)	< 0.1	0.1	< 0.1	< 0.1	< 0.1	< 0.1
Cs^+ (μg/L)	< 4	n. d.	< 4	n. d.	< 4	< 4
Rb^+ (μg/L)	< 10	n. d.	< 10	n. d.	< 10	< 10
Li^+ (mg/L)	< 0.01	< 0.01	< 0.01	< 0.01	< 0.01	< 0.01
Al^{3+} (mg/L)	0.28	0.35	< 0.2	0.22	< 0.2	0.22
Fe^{3+} (mg/L)	< 0.1	< 0.1	< 0.1	< 0.1	< 0.1	0.13
Mn^{2+} (mg/L)	< 0.1	0.1	< 0.1	< 0.1	< 0.1	< 0.1
Zn^{2+} (mg/L)	< 2.0	< 2.0	< 2.0	< 2.0	< 2.0	< 2.0

n.d.: not determined

The exchangeable cations in the samples are Ca^{2+}, Mg^{2+}, Na^+ and K^+ with minor amounts of Sr^{2+}, Ba^{2+}, Rb^+ and Cs^+ (Table 8- 3). Zinc is also present, although the presence of this cation is not very common. The order of abundance of these cations is $Ca^{2+} > Mg^{2+} > Na^+ > K^+ > Al^{3+} > Zn^{2+} > Sr^{2+} > Ba^{2+} > Rb^+ > Cs^+$, with some exceptions. For example, in samples KI0025F03; 51.9 m and KA2563A;154 m, potassium is more abundant than magnesium and sodium; and at KI0025F03; 73.1 m, 87.9 m and KI0025F;88.8 m, sodium is more abundant than magnesium.

The total cation exchange capacity is well correlated with the Al_2O_3 content (Figure 8-1) thus minerals such as illite and chlorite play an important role in the adsorption capacity of these samples. CEC values range from 31 to 44 μeq/g (Table 8- 3). These values are higher than others found in literature for the Finnsjö granite (≈ 3.2 μeq/g, Byegård et al., 1995) and for Grimsel mylonite (≈ 4.0 μeq/g, Bradbury, 1988). However, the obtained values are in the same order of magnitude of the

cation exchange capacity of Stripa Granite (≈ 17 µeq/g, Byegård, 1993) and Grimsel mylonite (≈ 19 µeq/g, Aksoyoglu, 1990). To check the consistency of the CEC data obtained for Äspö gouge fragments, other determinations were performed with the same method described by Byegård et al., 1995. However, no significant differences were found.

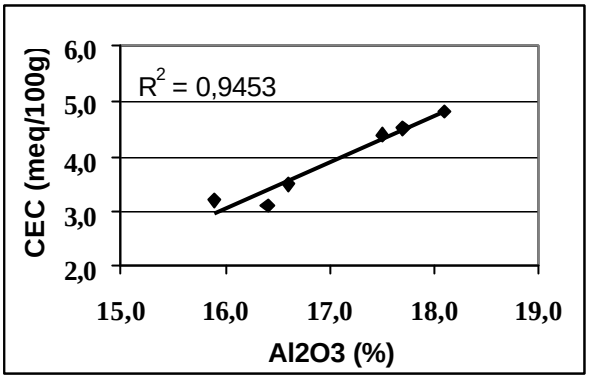

Figure 8- 1*. Correlation between CEC and Al_2O_3 of gouge fragments*

Table 8- 3 Cation exchange capacity obtained in the generic rock material

Sample	KI0025F03	KI0025F03	KI0025F03	KI0025F03	KI0025F	KA2563A
Depth (m)	**51.9**	**63.2**	**73.1**	**87.9**	**88.8**	**154**
Ca^{2+} (meq/g)	12.5	19.5	14.3	20.4	22.6	20.0
Mg^{2+} (meq/g)	7.0	11.5	5.5	6.4	7.2	2.7
Na^{+} (meq/g)	6.7	6.5	6.5	7.5	7.6	3.6
K^{+} (meq/g)	7.5	5.2	4.3	5.8	5.7	7.2
Al^{3+} (meq/g)	0.6	0.9	0.4	0.9	0.9	0.5
Zn^{2+} (meq/g)	0.2	0.1	0.1	0.1	0.2	0.3
Sr^{2+} (meq/g)	0.091	0.209	0.142	0.134	0.178	0.067
Ba^{2+} (meq/g)	0.080	0.056	0.028	0.0428	0.0497	0.086
Cs^{+} (meq/g)	0.000	0.001	0.0002	0.0008	0.0013	0.0004
Rb^{2+} (meq/g)	0.013	0.007	0.006	0.0258	0.0299	0.032
CEC Total (meq/g)	35	44	31	41	44	32

9 Comparison of physico-chemical parameters and CEC in the different structures

9.1 Structure # 6

This structure intersects KI0025F03 at 51.9 m and KA2563A at 154 m. The water adsorption of the gouge samples is 0.42% for KI0025F03: 51.9 m and 0.51% for KA2563A: 154 m. and the porosity is 1.08 % and 1.37 %, respectively. The higher porosity in KA2563A:154 m can be accounted for by the presence of fine-grained gouge material. The density is 2588 Kg/m^3 for KI0025F03: 51.9 m and 2725 Kg/m^3 for KA2563A: 154 m. This difference in density is mainly due to mineralogical differences. Thus, the low density obtained at 51.9 m can be due to the high content of feldspar and low content of Fe-bearing minerals compared with the rest of the samples. The total exchange capacity is 35 μeq/g for KI0025F03: 51.9 m and 32 μeq/g for KA2563A: 154 m. The amounts of exchangeable cations are similar and Ca^{2+} and K^+ are the most abundant exchangeable cations in both samples.

9.2 Structure # 22

Structure # 22 intersects KI0025F03 at 63.2 m and KI0025F at 88.8 m. The water adsorption of the gouge samples is 0.65% for the former and 0.72% the latter. The porosity in both samples is similar, 1.84% at 63.2 m and 1.92% at 88.8 m. The density is 2891 Kg/m^3 for KI0025F03: 63.2 m and 2719 Kg/m^3 for and KI0025F: 88.8 m. The highest density of all the samples is at KI0025F03: 63.2 m. This sample shows high Fe and Ca contents (Table 4- 1), compared to the other samples, which can account for the presence of high density minerals, like Fe-bearing minerals and, partially, for the existence of abundant epidote, respectively. The total exchange capacity and the exchangeable cations are similar for both samples (44 μeq/g).

9.3 Structure # 20

Structure # 20 is identified in KI0025F03 at 73.1 m. The water adsorption of the gouge sample is the lowest, 0.26%, as well as the porosity, 0.71%. The density is 2765 Kg/m^3, which is congruent with the existence of epidote and Fe-bearing minerals, as well as with its chemical composition, since both Ca and Fe contents are high. The total exchange capacity is 31 μeq/g.

9.4 Structure # 13

Structure # 13 cuts borehole KI0025F03 at 87.9 m. The water adsorption of the gouge sample is 0.78% and the porosity 2.05%. The density is 2683 Kg/m^3 and the total exchange capacity is 41 μeq/g. This sample presents the highest water adsorption and porosity of all the samples studied, as well as the highest exchange capacity. Most probably, these parameters are related to the high phyllosilicate content (Table 5-2). On the other hand, the density value is in agreement with a low content of epidote (Table 5-2) and moderate amount of Fe-bearing minerals, as the Fe content would imply (Table 4- 1).

10 Conclusions

- The mineralogical and textural heterogeneity of the fracture infilling material has been confirmed. Gouge fragments usually show approximately the same texture and mineralogy as the rock, though there can be different types of gouge fragments within the same sample. For example, the natural fine-grained gouge (<0.063 mm) taken in sample KA2563A-154 m has a very high content of feldspars and quartz, whereas among its gouge fragments (>1mm), there were some feldspar-quartz-rich fragments and others mineralogically and texturally similar to the Äspö diorite.

- The high contents of CaO in KI0025F03 at 63.2 m and 73.1 m are, in part, due to the formation of epidote from alteration of biotite. Chloritization of biotite is complete.

- The presence of barite, cromite, zircon, and several sulphides, such as, sphalerite, galena, pyrite and chalcopyrite account for Ba, Cr, Zr, Zn, Pb, Fe, Cu, respectively. U is scarce as expected, and U oxide associated with silicates has been observed as traces in coatings.

- Saponite has been found in scarce amounts in KI0025F03 at 87.9 m, which indicates that swelling clays are present, though their amount may be biased by drilling.

- Calcite crystals overlying coatings are considered as recently precipitated based on textural relationships. They have been precipitated at ambient temperatures and from a mixture of precipitation and glacial melt water according to the signatures of ^{13}C and ^{18}O. However, a hydrothermal origin should not be ruled out, since the dissolution and reprecipitation of old carbonates with high $\delta\ ^{13}C$ values can still have a hydrothermal signature left in the C sources.

- The $^{234}U/^{238}U$ activity ratio is approximately 1, except in KI0025F03 (63.2 m) in which it is less than unity. Consequently, ^{238}U is in equilibrium with ^{238}U, in the first case, and in the second case, a slow leaching of ^{234}U is assumed, so that ^{230}Th is supported by the ^{234}U that remains. An uptake of U in equilibrium is also observed, based on the $^{230}Th/^{234}U$ and $^{230}Th/^{238}U$ AR. Ra is being accumulated.

- Density is fundamentally related to the contents of Fe and Ca, which mineralogically, are represented by Fe-bearing minerals, and partially, by epidote, respectively.

- The highest water adsorption, porosity and CEC can be related to the highest contents of phyllosilicates.

Acknowledgement

This work was funded by ENRESA. We want to thank the Chemical Department for the chemical analyses, and specifically Dr. Miguel Sánchez for the corroboration of certain analyses and the Environmental Impact of Energy in CIEMAT for the determination of the radioactive isotope data. We are also grateful to Dr. Angel LaIglesia from CSIC for the XRD, Pedro Sánchez for the thin sections and Francisco Orden for the preparation of the samples. We also want to thank Dr Anders Winberg and Dr. Eva-Lena Tullborg for thier helpful comments.

References

Aksoyoglu S. (1990). Cesium sorption on mylonite. Journal of radioanalytical and Nuclear Chemistry, Articles, Vol. 140 nº 2, pp. 301-313.

Bradbury M. H. (1989). Laboratory investigations in supports of the migration experiments. Nagra Technical report 88-23.

Byegård J. (1993): The possibility of using slightly sorbing cations in tracer experiments in the Äspö hard rock laboratory. A literature survey and some basic considerations. SKB progress report 25-93-14.

Byegård J., Skarnemark G. And Skålberg M. (1995): The use of some ion-exchange sorbing tracer cations in *in situ* experiments in high saline groundwaters. Mat. Res. Soc. Symp. Proc. Vol. 353, pp 1077-1084.

Deer, W.A., Howie, R.A., Zussman, J. (1962): Rock forming minerals. Vol 1: Ortho and ring silicates. Longmans.

Deutsche Norm DIN-52103, Verfahren A: Bestimmung von Wasseraufnahme aun Sättigungswert. Oktober 1988.

Elliasson,T. (1993): Mineralogy, geochemistry and petrophysics of red coloured granite adjacent to fractures. SKB Technical Report 93-06.

Procedure for the determination of U isotopes in soils by alpha spectrometry (PR-X2-09). CIEMAT´s quality control procedure.

Procedure for the determination of ^{230} Th in soils (PR-X2-01). CIEMAT´s quality control procedure.

Procedure for the determination of the cation exchange capacity (IMA/X8/BI-Q6). CIEMAT´s quality control procedure.

Reyes, E., Delgado, A., Caballero, E., Núñez, R. & Cortecci, G. (2000): Estudio isotópico de las aguas y las alteraciones hidrotermales y meteóricas de "El Berrocal". CSIC-El Zaidín, Granada. Interim report.

Rhoades, J. D. (1982): Cation Exchange Capacity. In: Methods of Soil Analysis, Part 2. Chemical and Microbiological Properties. Agronomy Monograph Nº 8 (2nd edition). ASA-SSSA, 677. WI53711. USA.

Säfvestad, Anna; Andersson, Christina (1999). Detailed characterisation stage water-sampling campaign class 2, WBS 3.3.1.2. ITD-99-28. TRUE Block Scale project. Äspö Hard Rock Laboratory.

Stanfors, R., Rhén, I., Tullborg, E-L., Wikberg, P. (1999): Overview of geological and hydrogeological conditions of the Äspö hard rock laboratory site. Applied Geochemistry 14, 819-834.

Thomas, G.W. (1982): Exchange cations. In: Methods of Soil Analysis, Part 2. Chemical and Microbiological Properties. Agronomy Monograph Nº 9 (2nd edition). ASA-SSSA, 677. WI53711. USA.

Tullborg, E-L., Wallin, B. (1991): Stable isotopes studies of calcite fracture fillings (^{18}O, ^{13}C) and groundwaters (^{18}O, D). In: Tullborg, E-L., Wallin, B., Landström, O. (Eds.), Hydrogeochemical studies of fracture minerals from water conducting fractures and deep groundwaters at Äspö (special issue). SKB PR 25-90-01, 1-24.

Tullborg, E-L., Landström, O., Wallin, B (1999a): Low-temperature trace element mobility influenced by microbial activity--indications from fracture calcite and pyrite in crystalline basement. Chemical Geology 157, 199-218.

Tullborg, E-L (1999b): Status report on mineralogical and geochemical description of features #6, #13, #20, #9 and #19. TRUE Block Scale Project. June 1999.

Wallin, B and Peterman, Z. (1999): Calcite fracture fillings as indicators of paleohydrology at Laxemar at the Äspö Hard Rock Laboratory, southern Sweden. Applied Geochemistry 1144, 953-962.

ANNEX A

Original rocks

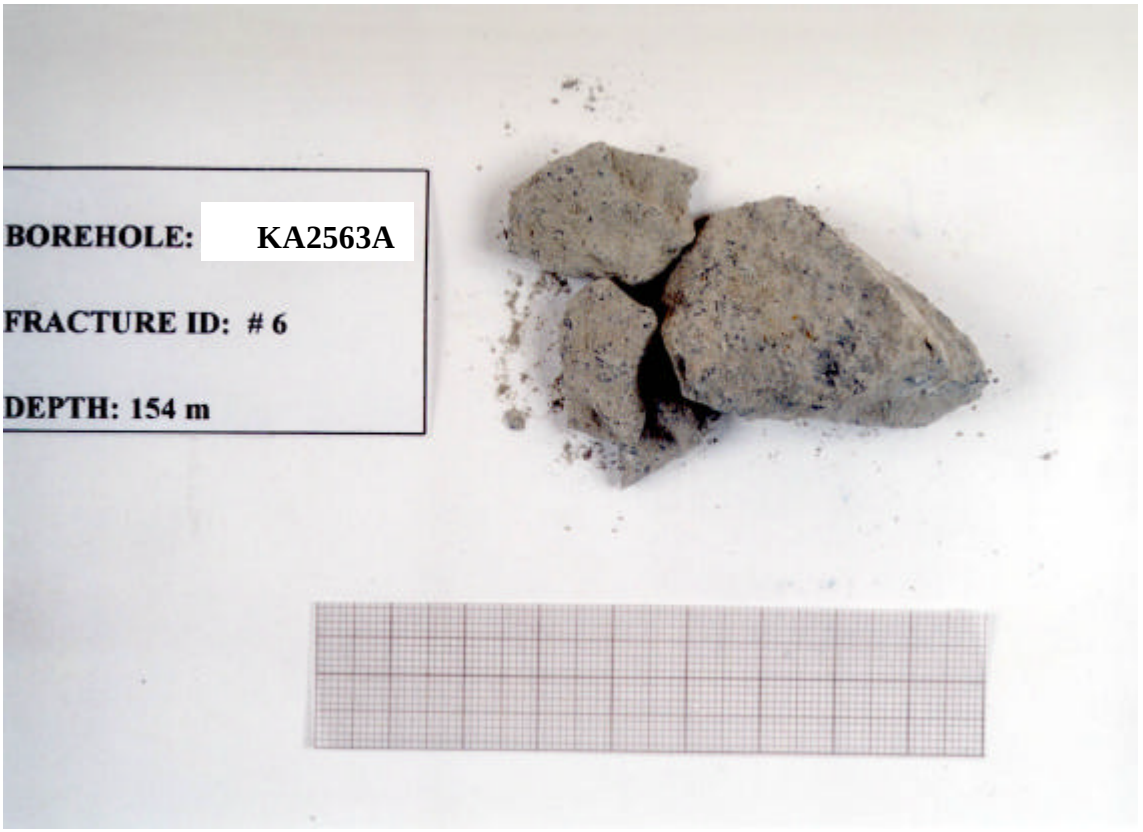

Fig. 1

Fig. 2

Fig. 3

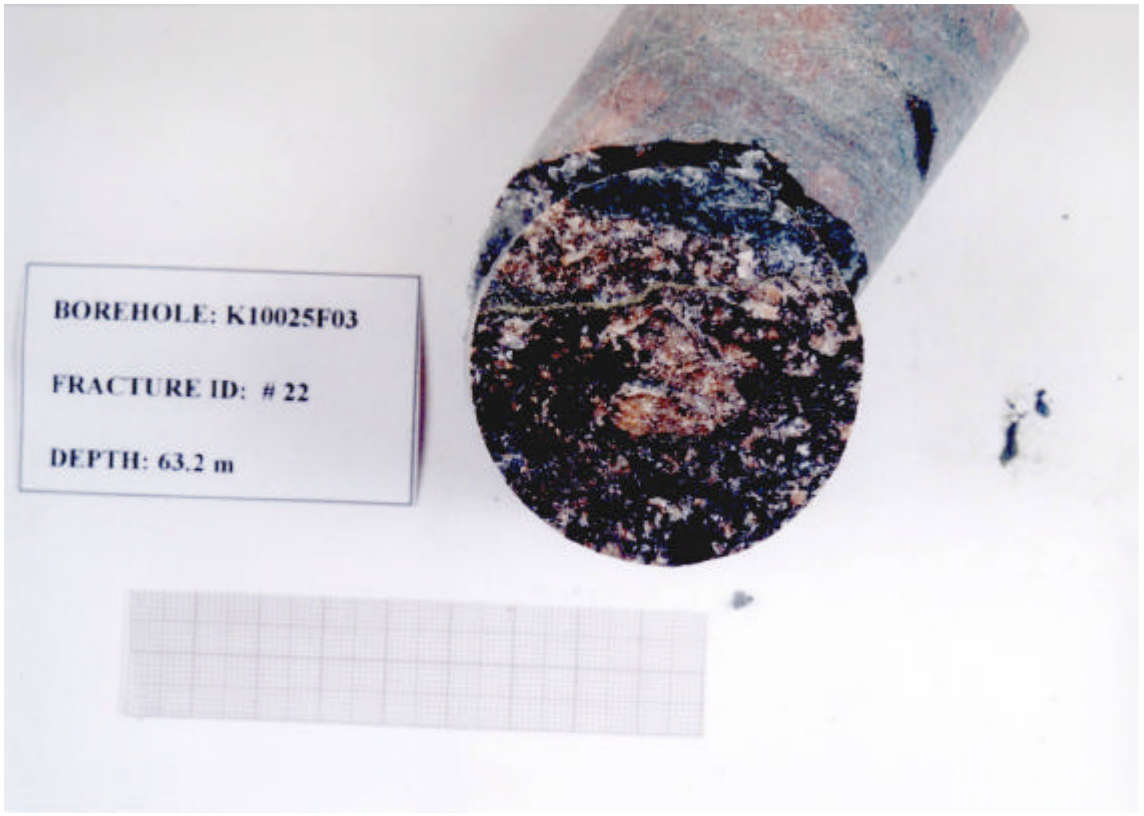

Fig. 4. Detail of calcite coating

Fig. 5

Fig. 6. Calcite macrocrystal in coating

Fig. 7

Fig. 8

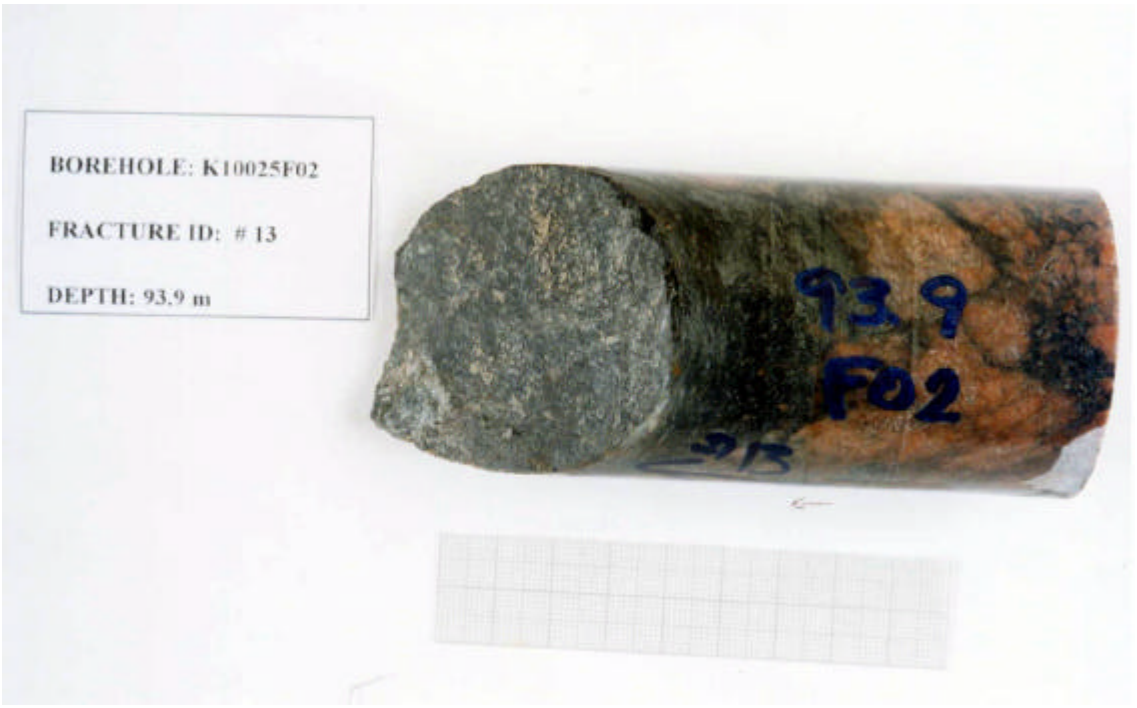

Fig. 9

ANNEX B

Petrographic microphotographs

ANNEX B
Fig. 1. BOREHOLE KI0025F03/ 51.9m / #6

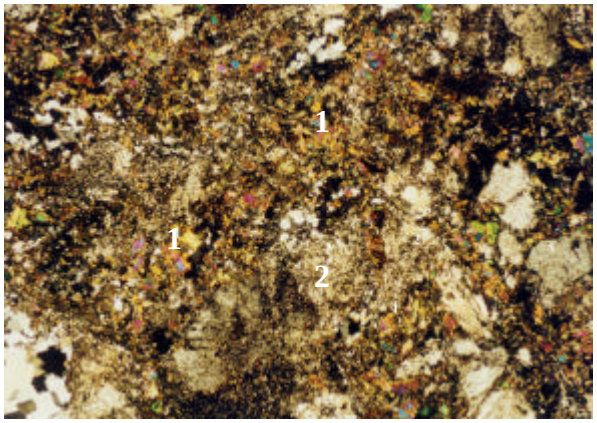

a Rock

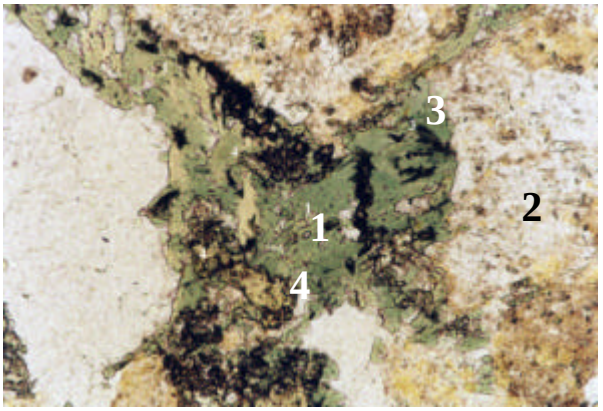

b Rock

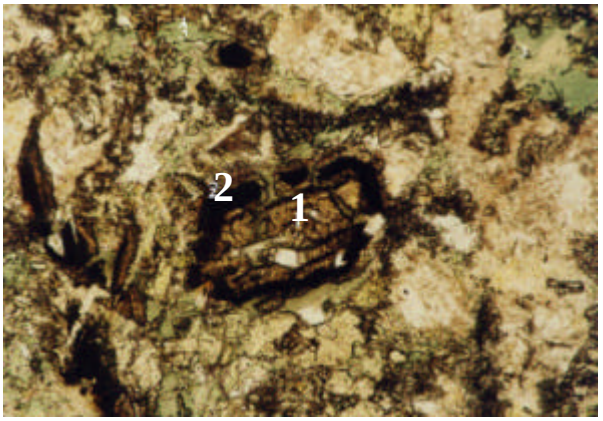

c Rock

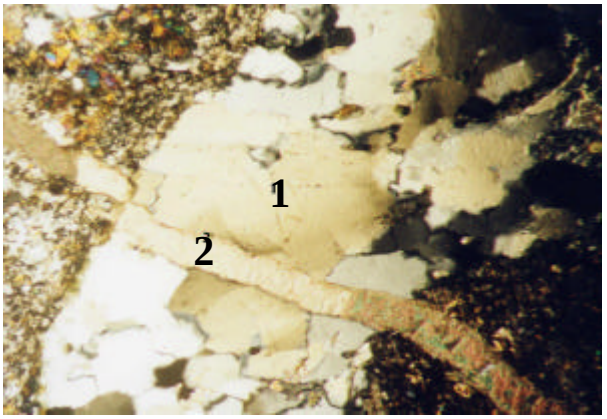

d Gouge

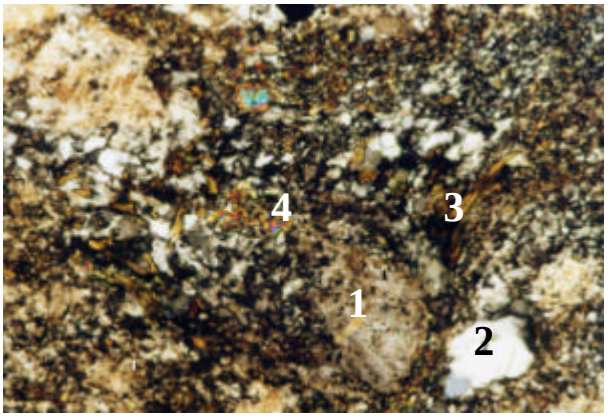

e Gouge

a) General aspect of cataclastic Äspö diorite: 1) epidote; 2) plagioclase. Crossed nicols, x12. **b)** Biotite totally altered to chlorite (1) with opaques (3) from biotite along cleavages; epidote (4) associated with chlorite. Plagioclase (2) slightly altered to sericite. Natural light, x100. **c)** Idiomorphic sphene (1) with alteration rims of Ti oxide (anatase, 2). Chlorite (3). Crossed nicols, x50. **d)** Fissural calcite (2) cutting recrystallized quartz (1). Crossed nicols, x50. **e)** General aspect of gouge fragment. Sericitized plagioclase (1), recrystallized quartz (2), chlorite (3) and epidote (4). Crossed nicols, x50.

ANNEX B

Fig. 2. BOREHOLE KA2563A / 154m / #6

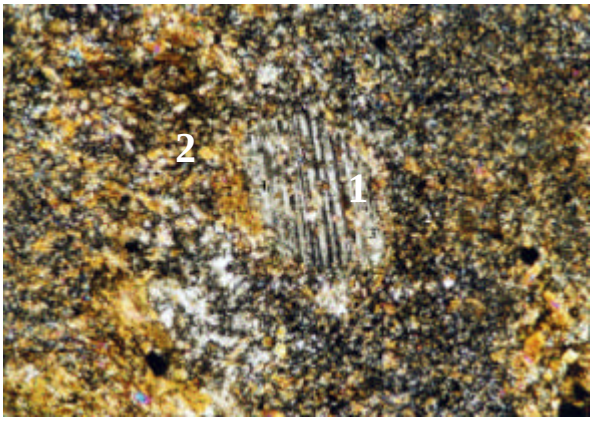

a

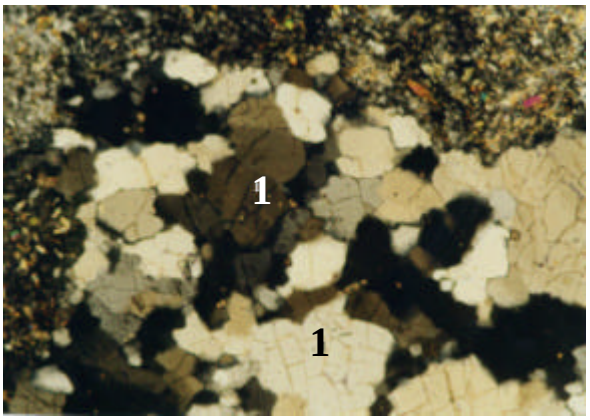

b

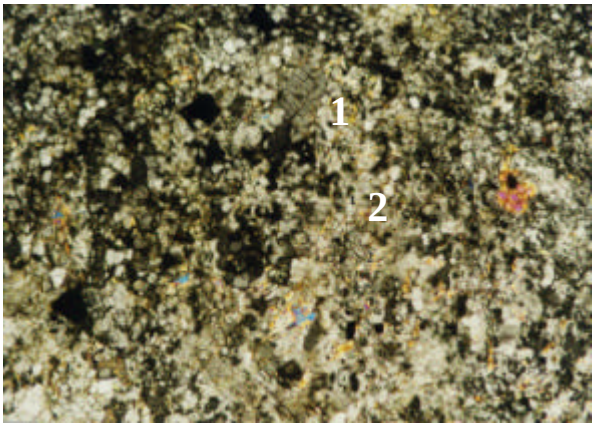

c

Gouge fragments. a) General aspect. Plagioclase (1). Fine-grained epidote-chlorite (2). Crossed nicols, x50; **b)** Lenticle of recrystallized quartz (1). Crossed nicols, x50. **c)** Altered Na-Ca plagioclase (1, only flakes of sericite (2) remain in some plagioclases). Crossed nicols, x50.

ANNEX B

Fig. 3. BOREHOLE KI0025F03/ 87.5m / #13

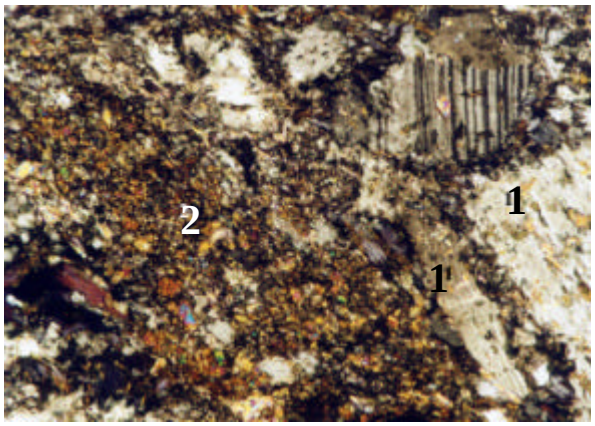

a **Rock**

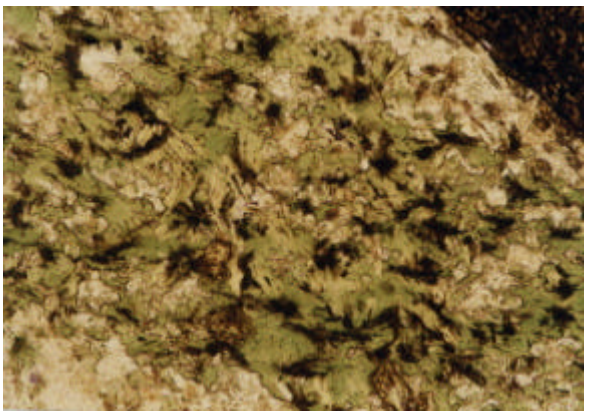

b Rock

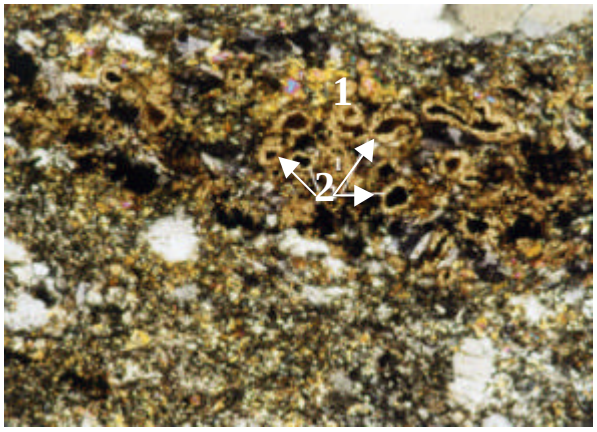

c Rock

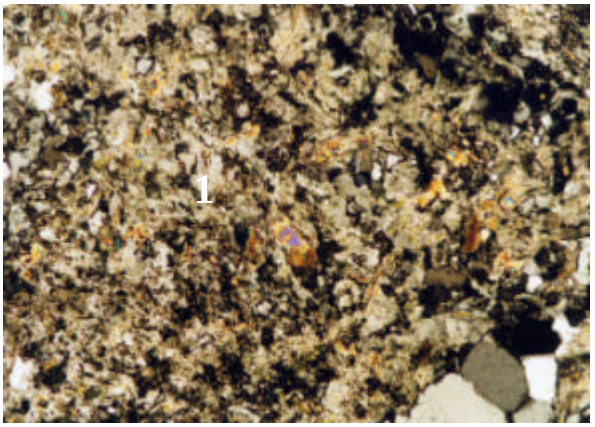

d Gouge

a) General aspect of tectonized zone with slightly altered plagioclase (1). Bands of epidote-chlorite (2) are observed. Crossed nicols, x50. **b)** Chlorite formed by alteration of biotite. The heavy metal inclusions of biotite are still observed along the cleavage planes. Crossed nicols, x50. **c)** Zone (1) of opaques and Ti oxides surrounded by carbonate halo (2). Crossed nicols, x50. **d)** Gouge fragment showing altered plagioclase (1), in which only sericite flakes (yellow) remain in some of them. Crossed nicols, x50.

ANNEX B

Fig. 4. BOREHOLE KI0025F02/ 93.9 m/ #13

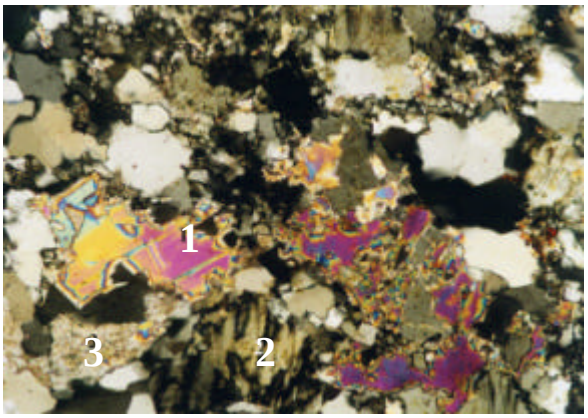

a Rock

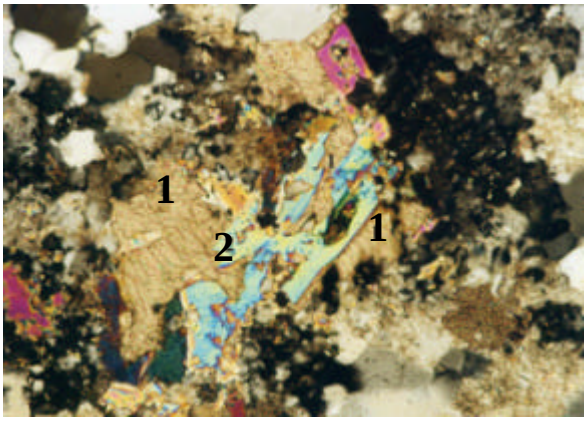

b Rock

a) General aspect of mylonite. K-feldspar (2), plagioclase (3) and poikilitic muscovite (1) are the main minerals. Crossed nicols, x50. **b)** Calcite (1) fills void and replaces muscovite (2). Crossed nicols, x50.

ANNEX B
Fig. 5. BOREHOLE KI0025F03/ 63.2m / #22

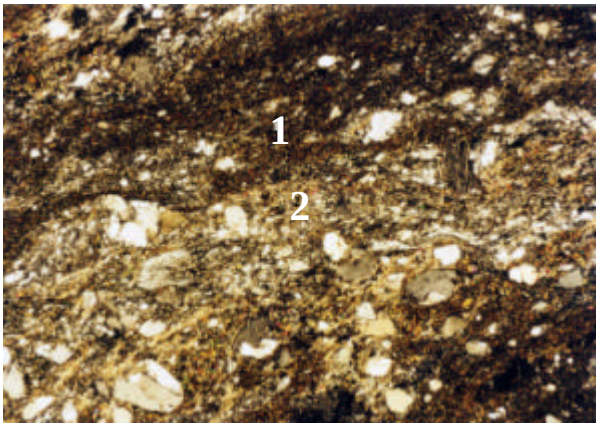

a Rock

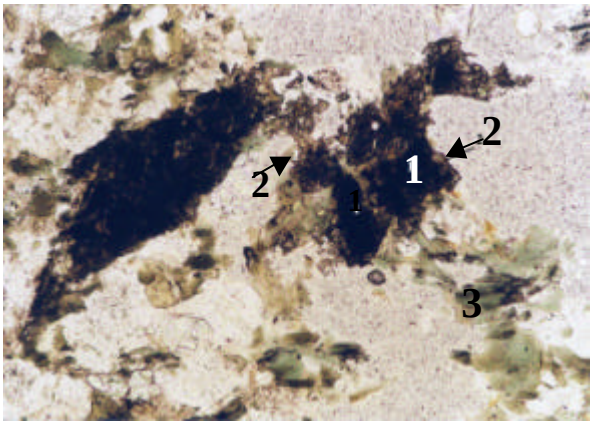

b Rock

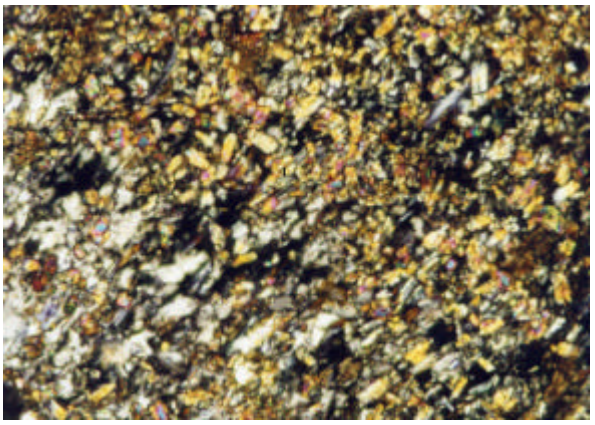

c Gouge

a) General aspect of a mylonite, fine-grained bands (1) alternating with coarser bands (2). Crossed nicols, x12; **b)** Opaques (1) surrounded by carbonates (2). Chlorite (3) formed by alteration of biotite. Natural light, x50; **c)** General aspect of a gouge fragment mainly formed by fine-grained idiomorphic-subidiomorphic epidote (bright yellow) and chlorite (brown spots), both from alteration of biotite. Crossed nicols, x50.

ANNEX B

Fig. 6. BOREHOLE KI0025F/ 88.8 m/ #22

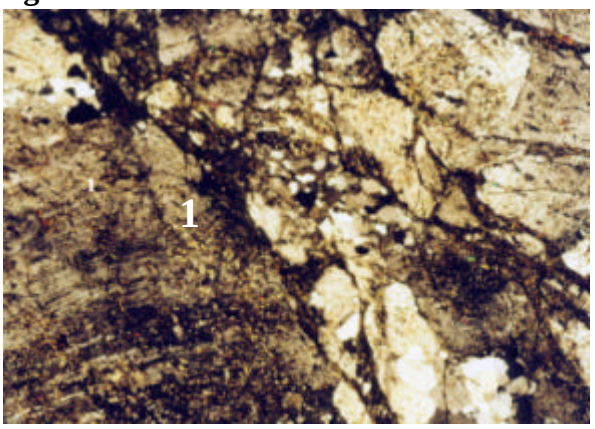

a Rock

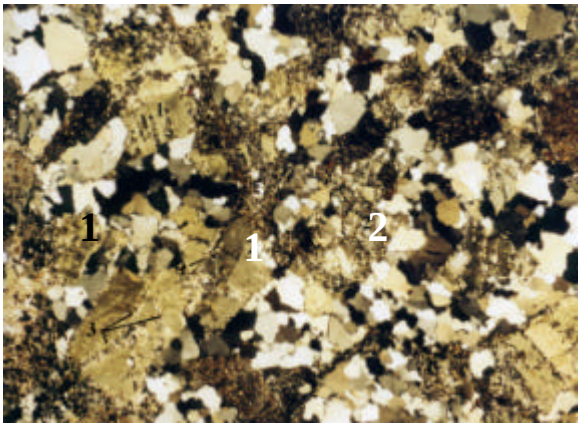

b Gouge

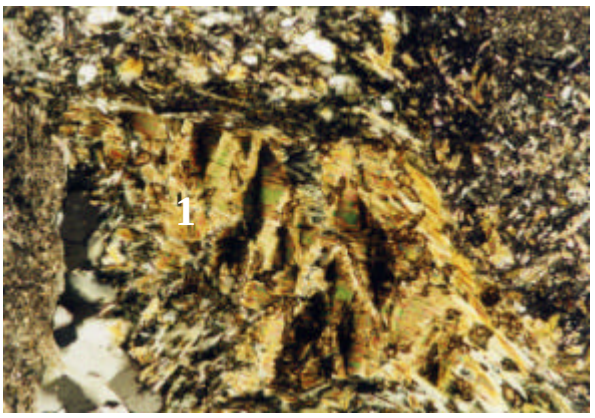

c Gouge

a) Äspö diorite with slightly sericitized plagioclase (1) macrocrystal. Crossed nicols, x12; **b)** General aspect of a gouge fragment with K-feldspars (1) and plagioclase (2). Crossed nicols, x12; **c)** Kinks (1) formed in chlorite (from alteration of biotite), indicating the strong deformation undergone by these rocks. Crossed nicols, x50.

ANNEX B
Fig. 7. BOREHOLE KI0025F03/ 73.1m / #20

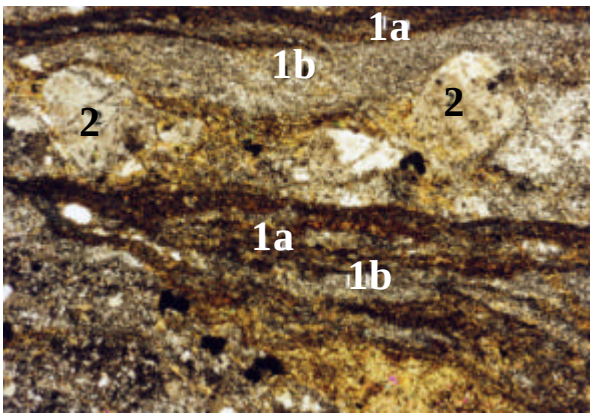

a Rock

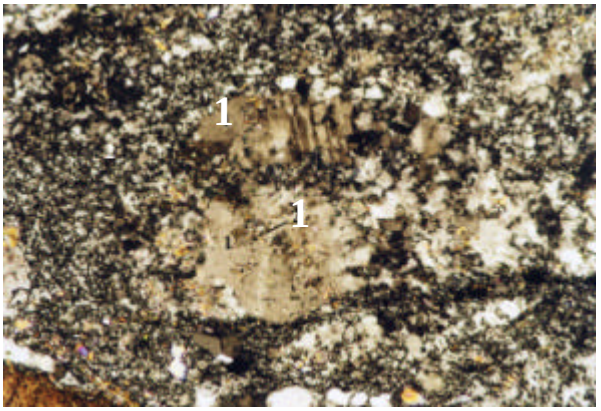

b Rock

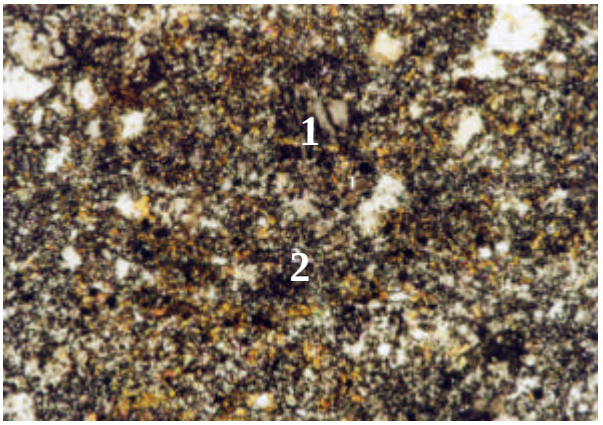

c Gouge

a) Fine-grained bands formed by epidote (1 a) and microcrystalline plagioclase (1b). These bands adapt themselves to plagioclase (2) macrocrystals. Frequent opaques. Crossed nicols, x12; **b)** Detail of plagioclase (1) in the coarser-grained bands. Crossed nicols, x50; **c)** General aspect of a gouge fragment. Plagioclase (1) and abundant epidote (2). Crossed nicols, x50.

ANNEX C

SEM microphotographs

ANNEX C

Fig. 1. BOREHOLE KI0025F03/ 51.9 m/ #6

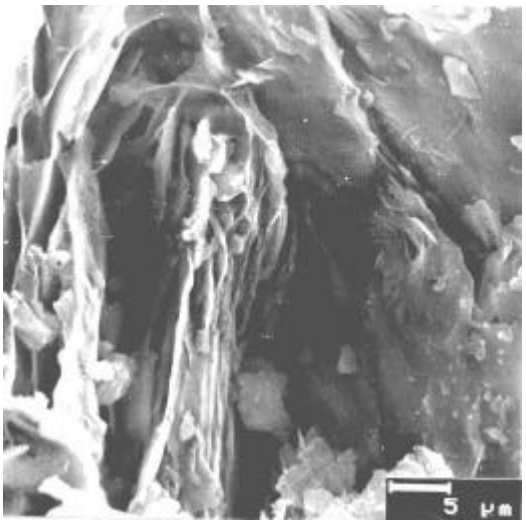

a) Chlorite in gouge

KA2563A/ 154m / #6

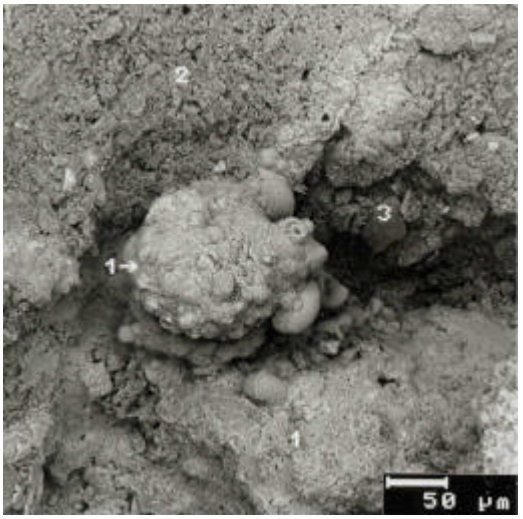

b) Gouge fragment. Collophorm Fe oxi-hydroxides (1) surrounded by a complex silicate compound with Mg, Ca and Fe (2). (1) and (2) have Cl probably from the evaporation of marine waters. Quartz (3).

Fig. 2. ANNEX C. KI0025F03/ 87.5 m/ #13. COATING

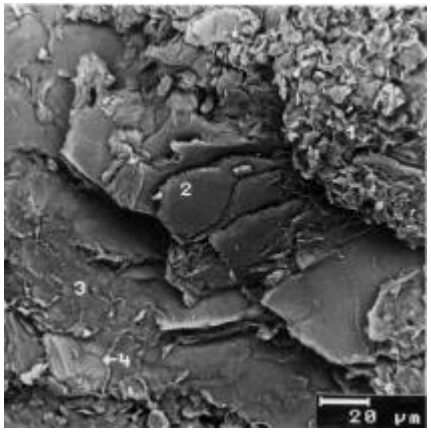

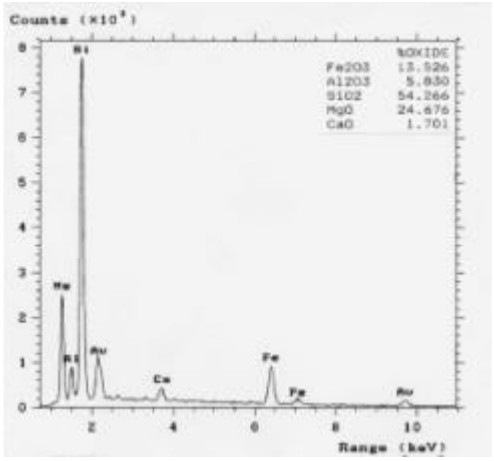

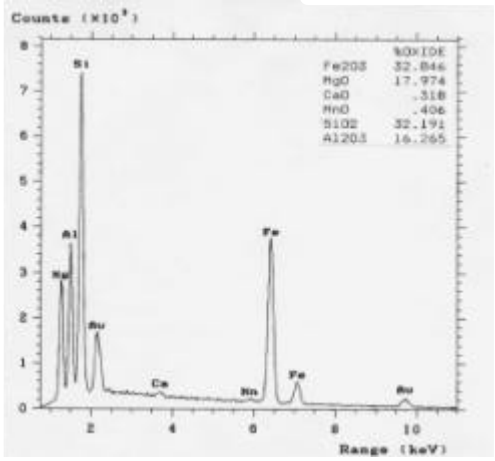

a. 1) saponite; 2, 3) chlorite; 4) apatite **a-1** **a-2**

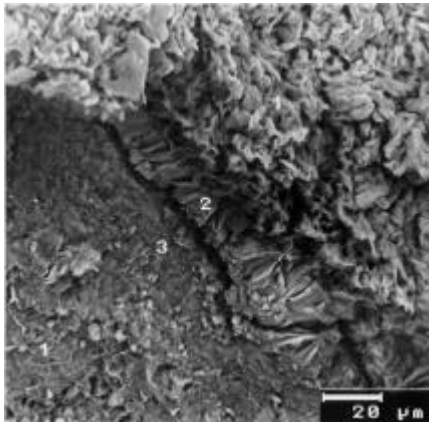

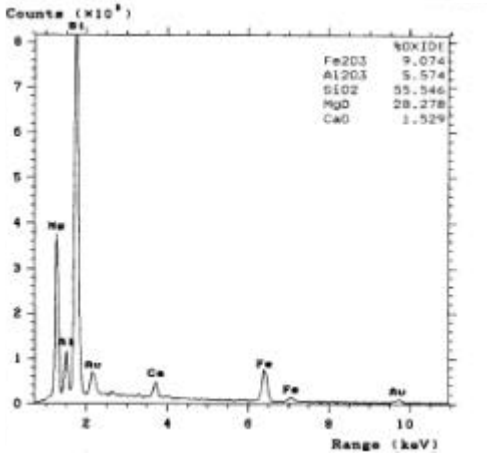

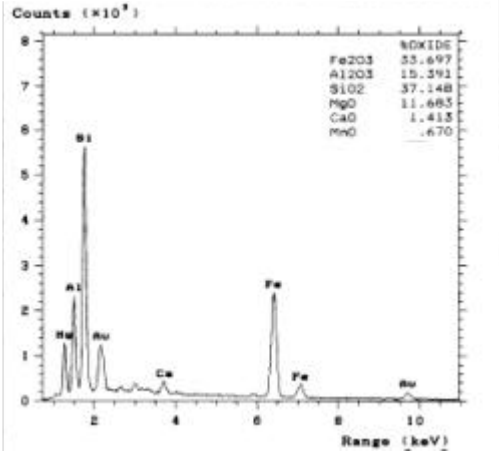

b. 1) saponite; 2) chlorite; 3) smectite **b-1** **b-2**

a, b) Chlorite tranformed into Mg-rich smectite (saponite). **a-1, b-1**: EDX spectrum of saponite; **a-2, b-2**: EDX spectrum of chlorite

Fig. 3. ANNEX C. KI0025F03/ 87.5 m/ #13. COATING

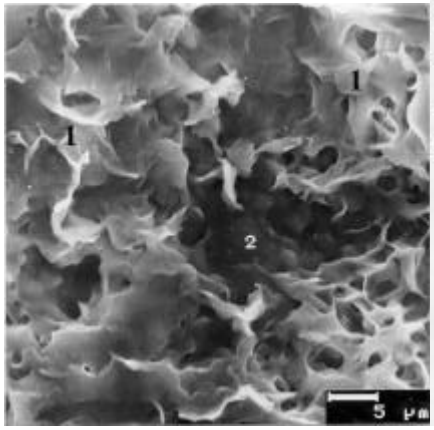

a. 1) saponite; 2) chlorite

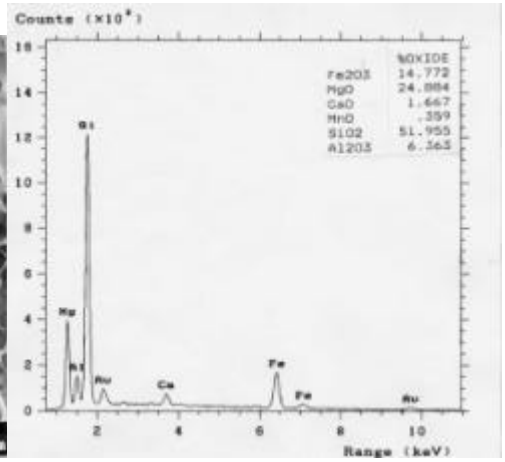

a-1. EDX spectrum of saponite

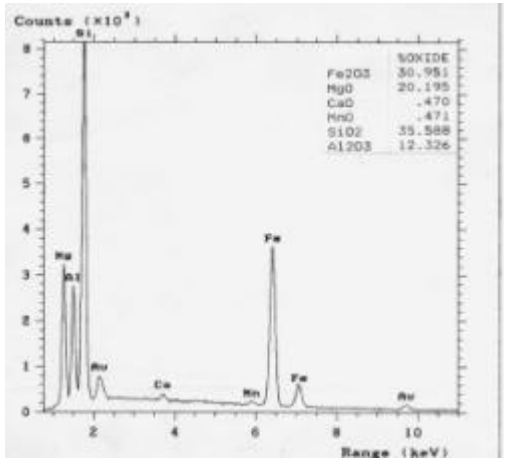

a-2. EDX spectrum of chlorite

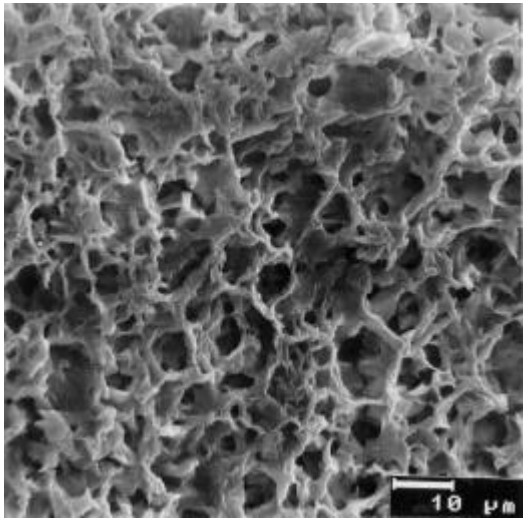

b . Saponite

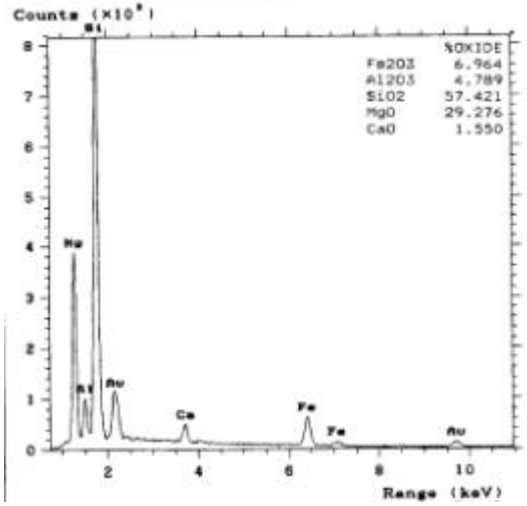

b-1. EDX spectrum of saponite

a) Chlorite altered to saponite**; b)** General aspect of saponite

Fig. 4. ANNEX C. KI0025F03/ 87.5 m/ #13. COATING

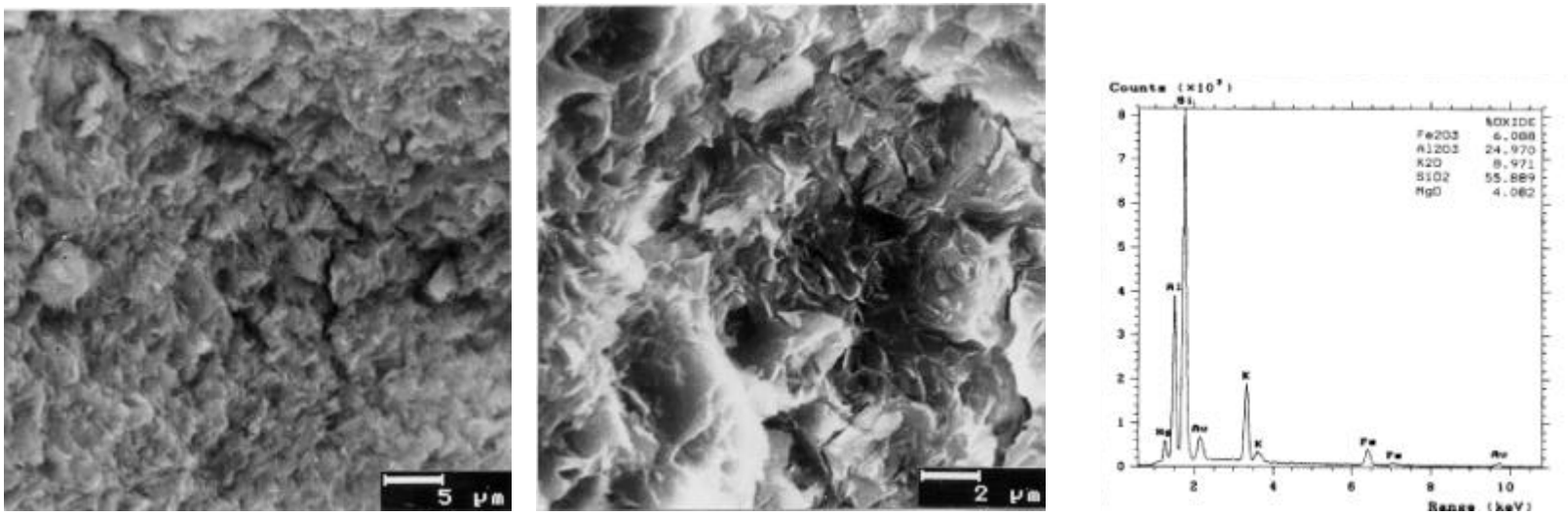

a **b** **c**

General aspect **(a)** and detail **(b)** of illite. **c)** EDX spectrum of illite

Fig. 5. **ANNEX C. KI0025F03/ 87.5 m/ #13. COATING**

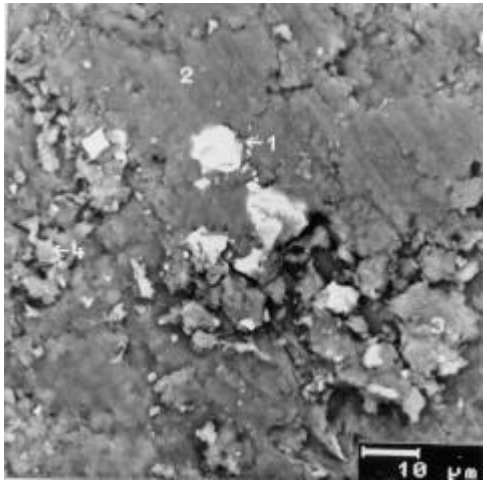

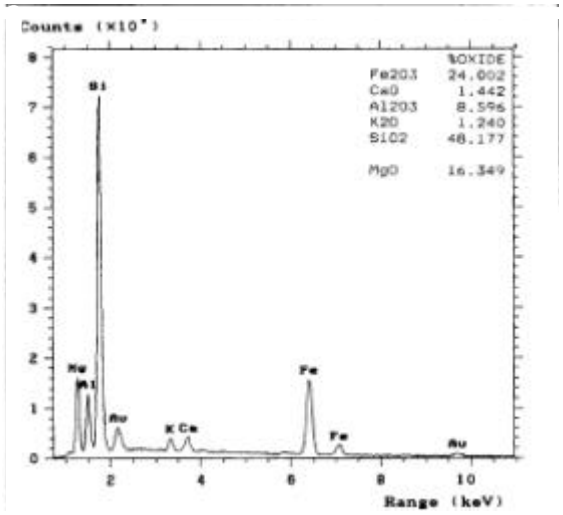

a. Pyrite (1) included in chlorite-calcite mass (2, 3); calcite (4)

a-1. EDX spectrum of chlorite-calcite

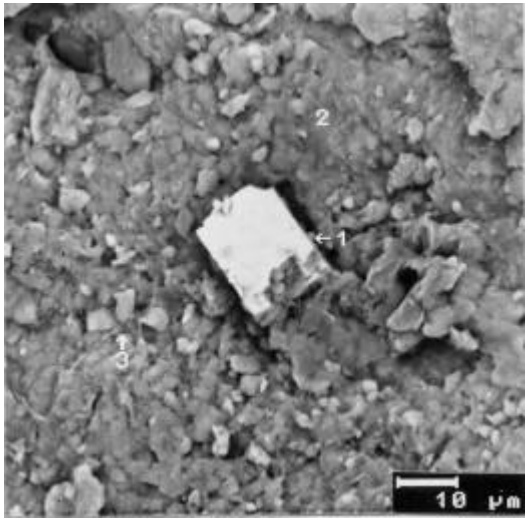

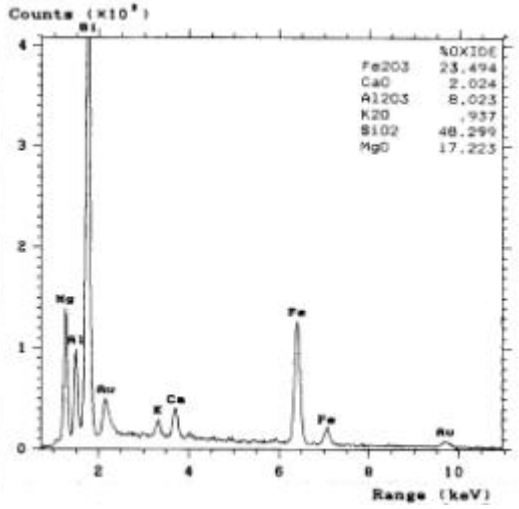

b-1

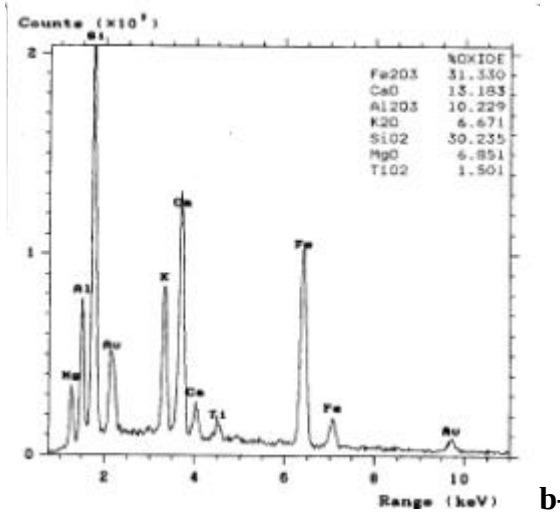

b-2

b) Pyrite (1) embedded in a mixture of biotite-calcite (3), which is partially transformed into chlorite-calcite (2); **b-1, b-2**: EDX spectrum of (2) and (3)

Fig. 6. ANNEX C. KI0025F02/ 93.9 m/ #13. COATING

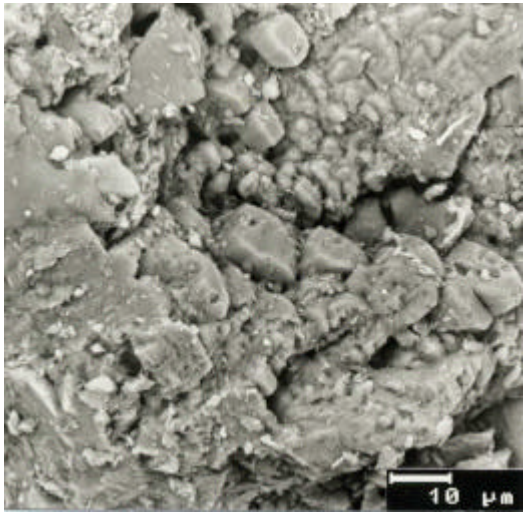

a. calcite

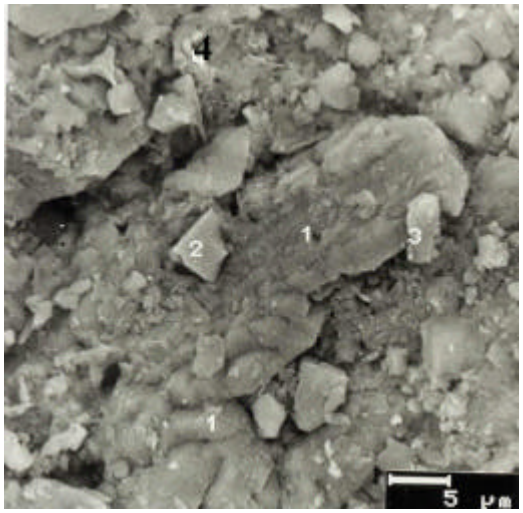

b. (1) calcite; (2) epidote; (3) K-feldspar; (4) chlorite

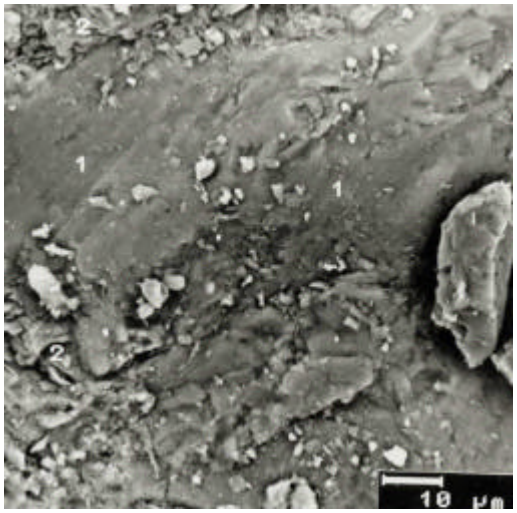

c. (1) K-feldspar + graphite; (2) biotite

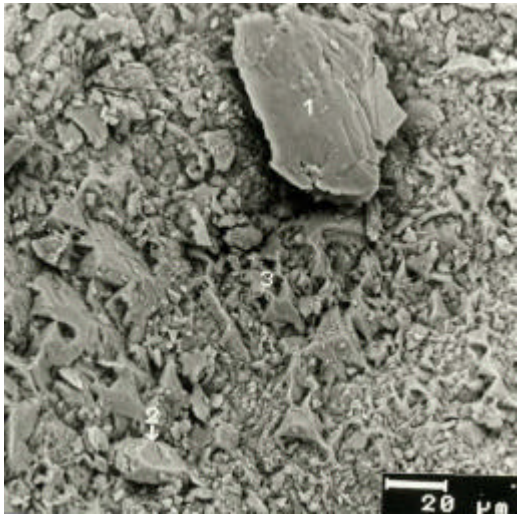

d. (1) plagioclase; (2) apatite; (3) calcite

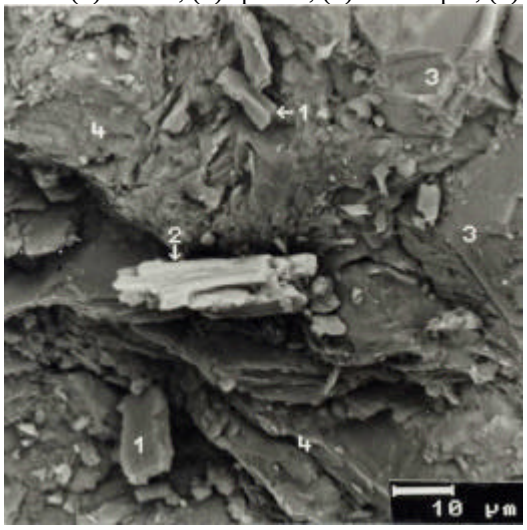

e. (1) quartz; (2) pyrite; (3) calcite; (4) muscovite-biotite

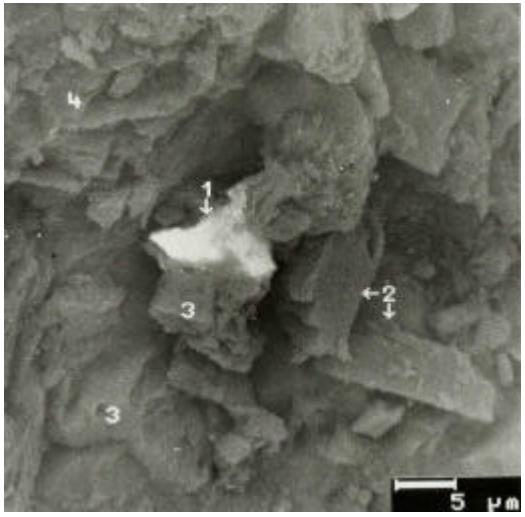

f. (1) U oxide (Pb); (2) K-feldspar; (3) epidote; (4) chlorite.

Fig. 7. ANNEX C. KI0025F03/ 88.8 m/ #22

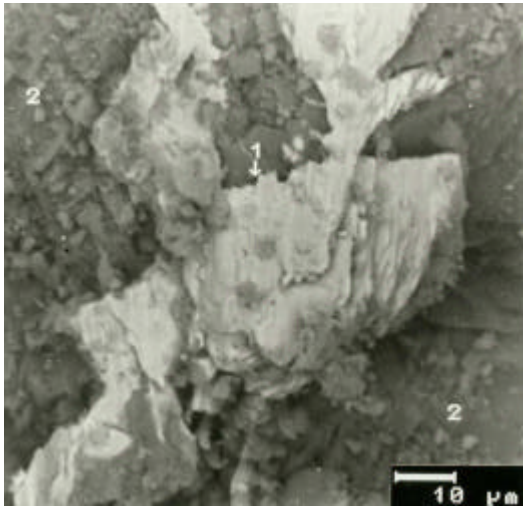

a. COATING. Cromite (1) and K-feldspar(2)

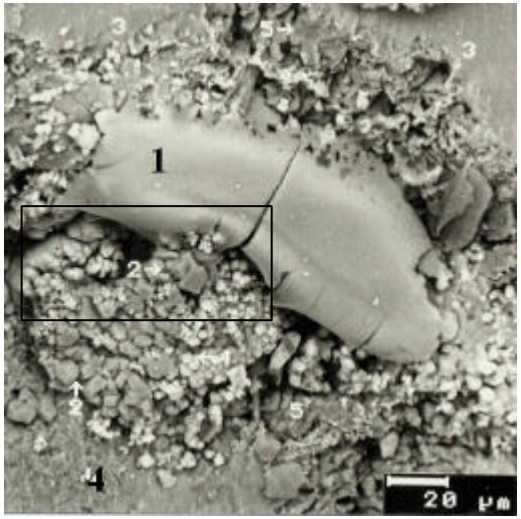

b. GOUGE. (1) Fe oxi-hydroxides; (2) calcite; (3) chlorite; (4) plagioclase; (5) quartz ; **c.** Detail aspect of **b**

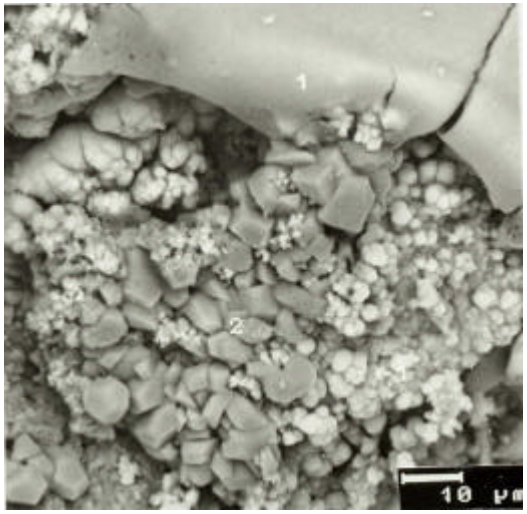

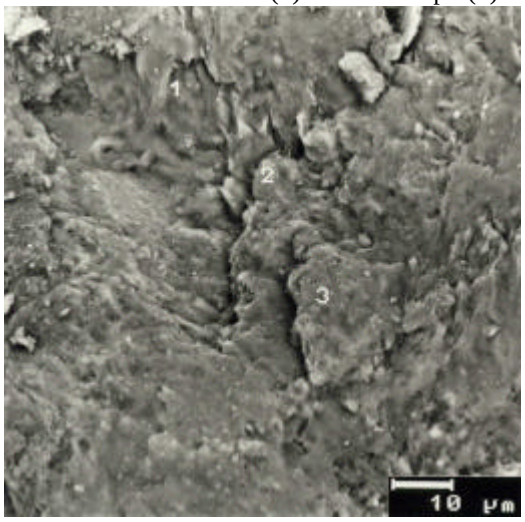

d. GOUGE. (1) biotite; (2) epidote; 3) sphene

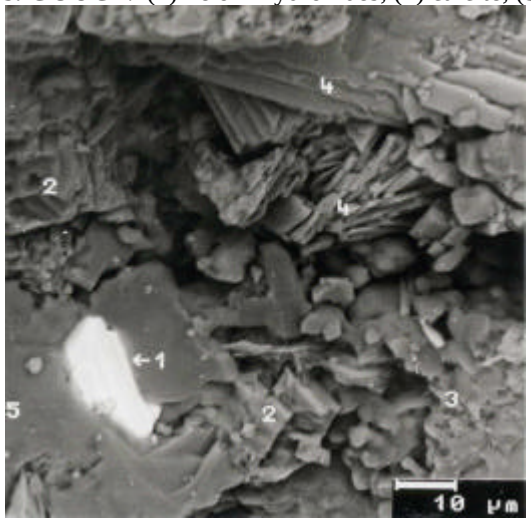

e. GOUGE. (1) chalcopyrite; (2) calcite; (3) plag; (4) epidote; (5) quartz

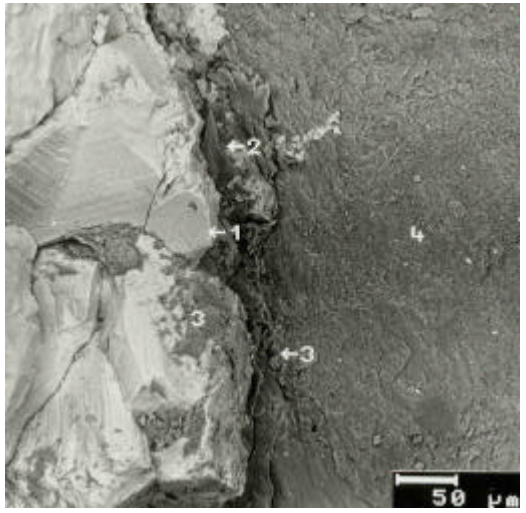

f. GOUGE. (1) pyrite; (2) quartz; (3) chlorite; K-feldspar

ANNEX C

Fig. 8. KI0025F03/ 73.1 m/ #22. GOUGE

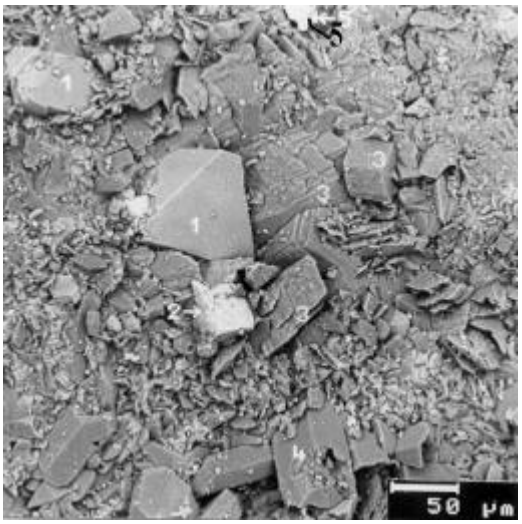

a

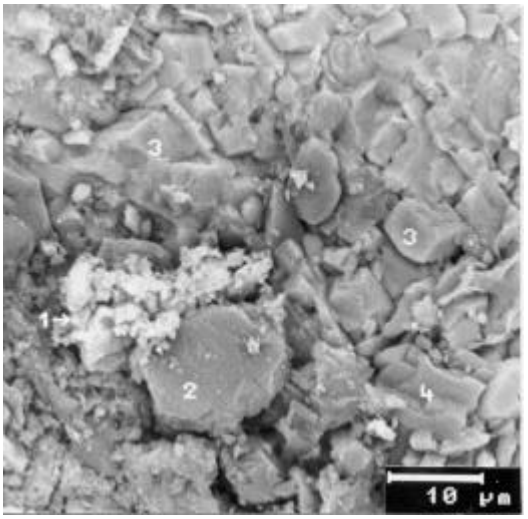

b

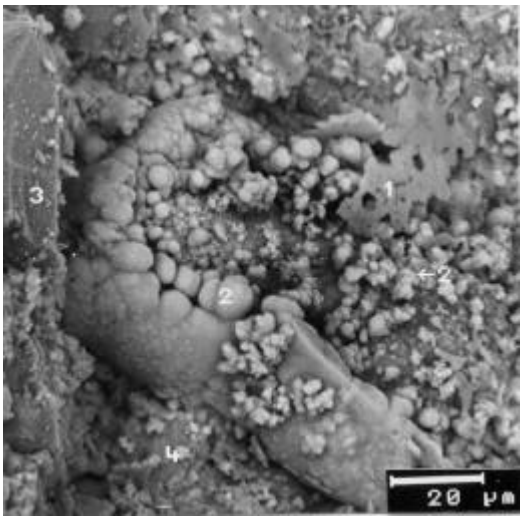

c

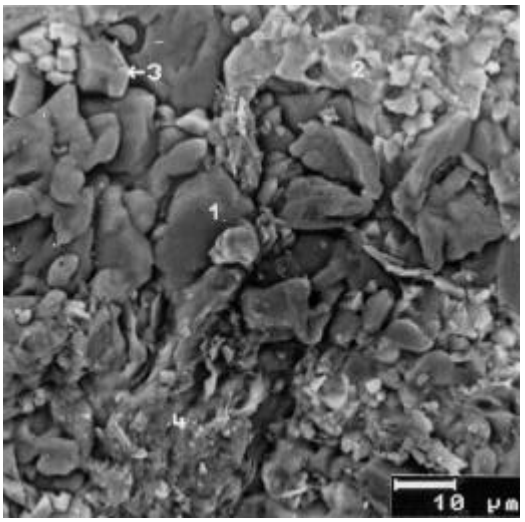

d

a. Idiomorphic fluorite (1), pyrite(2), K-feldspar (3), quartz (4), Fe oxi-hydroxide(5); **b.** Probable remobilization of zircon(1); chlorite (2) associated with epidote (3), Na-plagioclase (4); **c.** Collophorm Fe oxi-hydroxides (1, 2) with Cl from evaporation of groundwater, quartz (3) and epidote (4); d. Subidiomorphic quartz (1) with epidote and chlorite (2 and 4) and subidiomorphic plagioclase (3)

ANNEX C

Fig. 9. KI0025F03 / 87.5 m/ #13. GOUGE

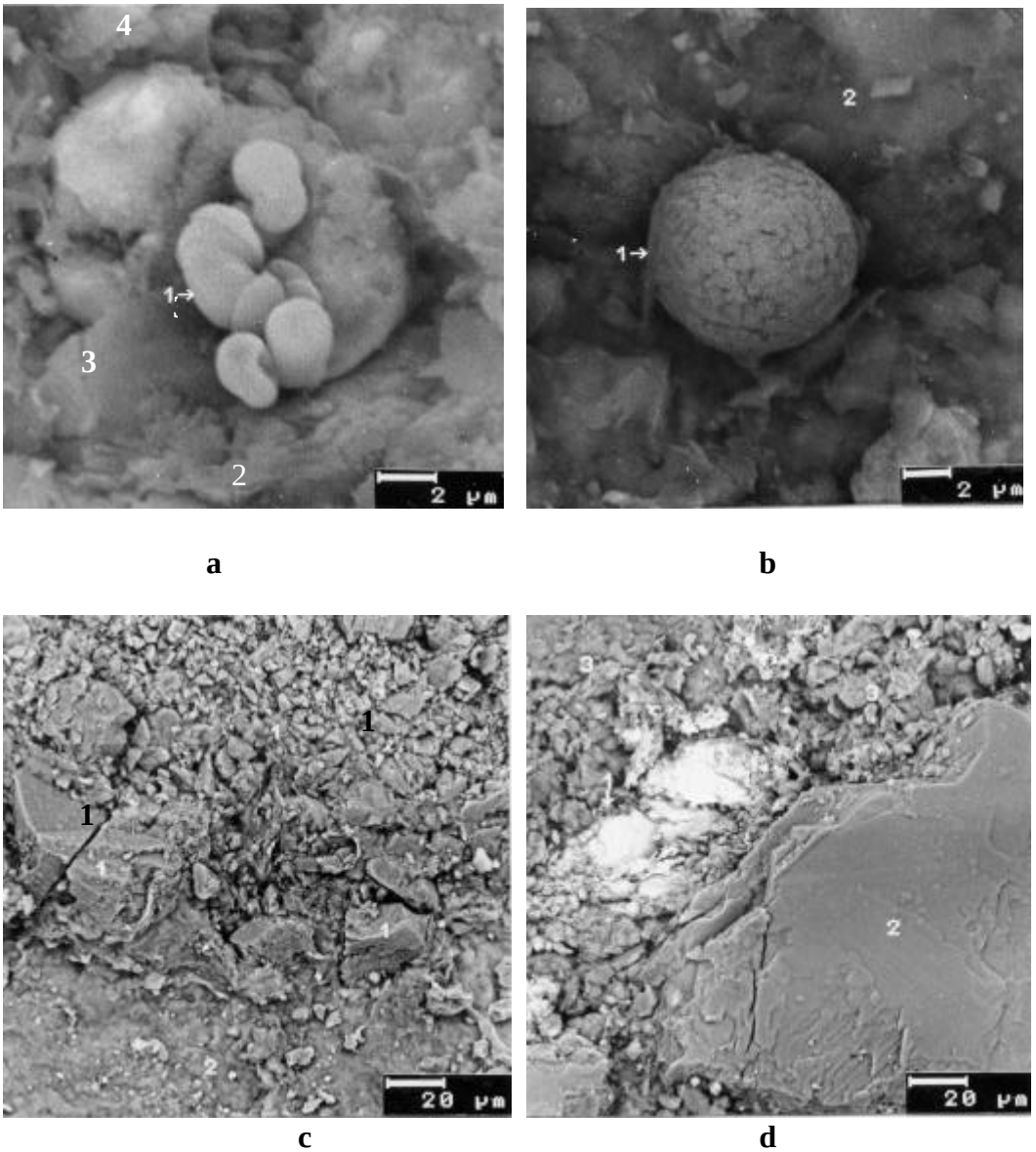

a **b**

c **d**

a) Spheres of Fe oxi-hydroxides (1) with plagioclase (2), epidote (3) and chlorite (4) and associated with biotite-chlorite (2) in **b.**
c) calcite (1) and chlorite (2); **d)** calcite (2) covering smectite (3), Zn oxides present (1)